TGFβ promotes low IL10-producing ILC2 with profibrotic ability involved in skin fibrosis in systemic sclerosis

Paôline Laurent, Benoit Allard, Pauline Manicki, Valérie Jolivel, Emeline Levionnois, Mohamed Jeljeli, Pauline Henrot, Julien Izotte, Damien Leleu, Alexis Groppi, et al.

OPEN ACCESS

TRANSLATIONAL SCIENCE

TGFβ promotes low IL10-producing ILC2 with profibrotic ability involved in skin fibrosis in systemic sclerosis

Paôline Laurent,[1] Benoit Allard ,[1] Pauline Manicki,[2] Valérie Jolivel,[1] Emeline Levionnois,[1] Mohamed Jeljeli,[3] Pauline Henrot,[2] Julien Izotte,[4] Damien Leleu ,[1] Alexis Groppi,[5,6] Julien Seneschal,[7,8] Joel Constans,[9] Carlo Chizzolini ,[10] Christophe Richez ,[1,2] Pierre Duffau,[1,11] Estibaliz Lazaro,[1,11] Edouard Forcade,[1,12] Thierry Schaeverbeke,[1,2] Thomas Pradeu,[1] Frédéric Batteux,[3] Patrick Blanco,[1,13] Cécile Contin-Bordes ,[1,13] Marie-Elise Truchetet [1,2]

Handling editor Josef S Smolen

► Additional supplemental material is published online only. To view, please visit the journal online (http://dx.doi.org/10.1136/annrheumdis-2020-219748).

For numbered affiliations see end of article.

Correspondence to
Pr Marie-Elise Truchetet, Rheumatology, CHU de Bordeaux, Bordeaux, Aquitaine, France;
marie-elise.truchetet@chu-bordeaux.fr

CC-B and M-ET contributed equally.

PL and BA are joint first authors.

Received 18 December 2020
Accepted 6 July 2021

To cite: Laurent P, Allard B, Manicki P, *et al*. *Ann Rheum Dis* Epub ahead of print: [*please include* Day Month Year]. doi:10.1136/annrheumdis-2020-219748

ABSTRACT

Objective Innate lymphoid cells-2 (ILC2) were shown to be involved in the development of lung or hepatic fibrosis. We sought to explore the functional and phenotypic heterogeneity of ILC2 in skin fibrosis within systemic sclerosis (SSc).

Methods Blood samples and skin biopsies from healthy donor or patients with SSc were analysed by immunostaining techniques. The fibrotic role of sorted ILC2 was studied in vitro on dermal fibroblast and further explored by transcriptomic approach. Finally, the efficacy of a new treatment against fibrosis was assessed with a mouse model of SSc.

Results We found that ILC2 numbers were increased in the skin of patients with SSc and correlated with the extent of skin fibrosis. In SSc skin, KLRG1^{-} ILC2 (natural ILC2) were dominating over KLRG1^{+} ILC2 (inflammatory ILC2). The cytokine transforming growth factor-β (TGFβ), whose activity is increased in SSc, favoured the expansion of KLRG1^{-} ILC2 simultaneously decreasing their production of interleukin 10 (IL10), which regulates negatively collagen production by dermal fibroblasts. TGFβ-stimulated ILC2 also increased myofibroblast differentiation. Thus, human KLRG1^{-} ILC2 had an enhanced profibrotic activity. In a mouse model of SSc, therapeutic intervention-combining pirfenidone with the administration of IL10 was required to reduce the numbers of skin infiltrating ILC2, enhancing their expression of KLRG1 and strongly alleviating skin fibrosis.

Conclusion Our results demonstrate a novel role for natural ILC2 and highlight their inter-relationships with TGFβ and IL10 in the development of skin fibrosis, thereby opening up new therapeutic approaches in SSc.

Key messages

What is already known about this subject?

- Type 2 innate lymphoid cells (ILC2) have emerged as a player in inflammatory and fibrotic processes.
- Research to date on innate lymphoid cells in systemic sclerosis (SSc) was descriptive suggesting a potential role in the disease development.
- Transforming growth factor-β (TGFβ) pathway is important in SSc pathophysiology notably through its direct role on fibroblasts.

What does this study add?

- We deeply described ILC2 presence and localisation in fibrotic skin.
- We depicted a new indirect mechanism by which TGFβ could lead to fibrosis, triggering the switch from an 'inflammatory' phenotype (KLRG1^{high}) to a 'natural' phenotype (KLRG1^{low}) ILC2.
- These TGFβ-activated ILC2, characterised by a diminished interleukin 10 (IL10) production, promote collagen synthesis by fibroblasts.
- Using both in vitro and in vivo models, we established the importance of the combined role of TGFβ and IL10 in the fibrotic process.

How might this impact on clinical practice or future developments?

- These data provide important support for the use of combination therapies in SSc.
- The combined use of an antifibrotic drug such as pirfenidone and IL10 could be a new therapeutic approach in this very complicated disease.

INTRODUCTION

Systemic sclerosis (SSc) is a systemic autoimmune disorder characterised by a dysregulated extensive fibrotic process that impacts epithelial barriers, within the gut, lung and skin.[1] Its pathogenesis remains poorly understood, and treatments for disease progression are limited. While the adaptive immune system has long been considered to be involved in SSc development, recent observations have established an important role of the innate immune system.[2 3] As an example, a type 2 macrophage signature has been identified in both skin and lung from patients with SSc.[4]

Interestingly, innate lymphoid cells (ILCs) that patrol environmental interfaces to defend against

infection and protect barrier integrity have emerged as crucial effectors in inflammatory and fibrotic diseases.[5 6] Their cytokine production and transcription factor expression allow the identification of three distinct subsets. Type 1 ILC (ILC1) are Tbet expressing cells that produce interferon-γ and tumour necrosis factor, and are dependent on IL12 and IL18 for their generation. GATA3 expressing type 2 ILC (ILC2), which are dependent on thymic stromal lymphopoietin (TSLP), IL25 and IL33 release IL5 and IL13 whereas type 3 ILCs (ILC3) express the transcription factor RORγt, release IL17 and IL22 and are generated after IL23 and IL1β stimulation.[7]

The role of ILC2 was first highlighted in allergic reactions.[8 9] More recently, murine studies have shown the role of ILCs in hepatic and pulmonary fibrosis, with a major effect of IL13 production. Interestingly in the context of SSc, TGFβ is another important profibrotic factor[10–12] and an essential cytokine for the development of ILC2,[13] suggesting a potential role of ILC2 on SSc pathogenesis.

To add another level of complexity, ILC2 constitute a heterogeneous population of cells and at least two separate clusters are described based on their differential responses to microenvironment. Inflammatory ILC2 (iILC2) respond to IL25 and produce IL17 in addition to IL13, whereas natural ILC2 (nILC2) respond to IL33 and release high levels of IL13. The differential expression of killer cell lectin-like receptor G1 (KLRG1) has been identified as a marker, with iILC2 being KLRG1^{+} and nILC2 being KLRG1^{-}. iILC2 can be considered a transient progenitor based on its ability to migrate to tissue and then differentiating into nILC2 in response to activation signals.[14 15] However, the relevance of this plasticity in human pathologies remains to be established.

In patients with SSc, we and others have demonstrated increased levels of homeostatic cytokines for ILC2, such as IL25, IL33 and TSLP.[16–18] Furthermore, our group found that TSLP is increased in the blood and skin of patients with SSc, with levels correlating to skin fibrosis.[18] In human SSc, the role of ILC2 remains elusive as only one observational study showed an increased proportion of circulating ILC2 at the blood and tissue level,[19] thus questioning the potential implication of ILC2 in the fibrotic process.

In our study, we demonstrate the potential role of ILC2 in the establishment of fibrosis in human SSc. We showed that KLRG1 expression on ILC2 was linked to the fibrotic stage of the disease. Mechanistically, in vitro and in vivo studies revealed that this switch operates in a TGFβ-dependent manner, leading to a decrease in IL10 production and a profibrotic phenotype. Interestingly, while pirfenidone alone (acting partly by the inhibition of TGFβ-induced effects) failed to significantly affect the fibrotic process in vivo, the addition of IL10 synergistically alleviated fibrosis. Overall, this study unravels a new role for ILC2 in fibrotic diseases and paves the way for new therapeutic strategies for human SSc.

METHODS

Materials and methods are described in the online supplemental file.

RESULTS

Number of circulating ILC2 is decreased in human SSc with the extent of skin fibrosis

To investigate the potential contribution of ILC2 in SSc pathogenesis, we first monitored the total ILC population and subpopulations in the whole blood of patients with SSc (SSc, n=73) and age-matched and sex-matched healthy donors (HDs) (n=59) (table 1).

The gating strategy to identify ILCs in the peripheral blood is described in the online supplemental figure 1A. The frequency and absolute numbers of ILCs (defined as Lin^{-} CD45^{+}CD127^{+}, figure 1A) were lower in SSc compared with HDs (0.04%±0.02% vs 0.09%±0.07%, p<0.0001 and 0.0009±0.0003 vs 0.002±0.001, p=0.0004; figure 1B and

Table 1 Demographic, clinical and biological characteristics of the SSc population

	Patients with lcSSc (n=50)	Patients with dcSSc (n=23)	All patients with SSc (n=73)	P value*
Female (%)	39 (78)	9 (40)	48 (65.8)	
Age at onset, mean±SD years†	48.7±13.2	49.9±14.5	49±13.5	ns
Disease duration, mean±SD years†	10.7±6.0	11.9±9.47	11.5±8.6	ns
RP (%)	50 (100)	23 (100)	73 (100)	ns
Digital ulcers (%)	20 (40)	7 (30.8)	27 (37)	0.02
mRSS, mean±SD	5.9±5.5	24.6±12.7	11.1±11.6‡	<0.0001
PAH (%)	7 (14)	1 (4.3)	8 (11)§	ns
Interstitial lung disease (%)	11 (22)	13 (56.5)	24 (32.9)¶	ns
Lung fibrosis (%)	7 (14)	1 (4.3)	8 (11)¶	ns
Renal crisis (%)	1 (2)	0 (0)	1 (1.4)¶	ns
Antinuclear autoantibody-positive	50 (100)	23 (100)	73 (100)	ns
Anticentromere antibody-positive	25 (50)	1 (4.34)	26 (35.6)	ns
Antitopoisomerase antibody-positive	4 (8)	11 (47.8)	15 (20.5)	ns
Anti-ARNIII polymerase antibody-positive	1 (2)	1 (4.34)	2 (2.7)	ns
Immunomodulatory agents	44 (22)	60.8 (14)	49.3 (36)	ns

Except where indicated otherwise, values are the number (%).
*lcSSc versus dcSSc.
†Age at onset of symptoms other than RP and disease duration since symptoms other than RP.
‡Data were available for 34 patients.
§Data were available for 36 patients.
¶Data were available for 35 patients.
dcSSc, diffuse cutaneous SSc; lcSSc, limited cutaneous systemic sclerosis; mRSS, modified Rodnan skin thickness score; ns, not significant; PAH, pulmonary hypertension; RP, Raynaud's phenomenon; SSc, systemic sclerosis.

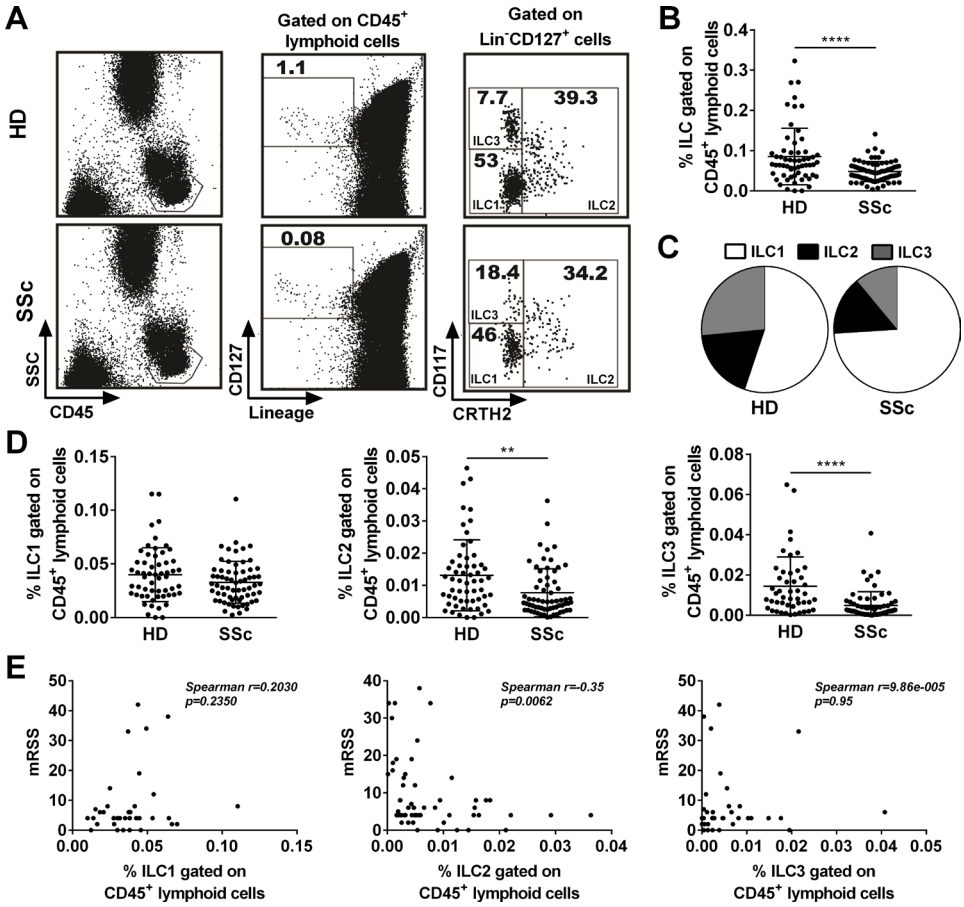

Figure 1 Characterisation of innate lymphoid cells (ILCs) in the blood of patients with systemic sclerosis (SSc) and healthy donors (HDs). (A) Representative dot plot of circulating ILCs in the HD and SSc blood samples and (B) ILC frequency quantification. (C) Proportion of ILC subsets in the blood from HDs and patients with SSc. (D) Percentage of circulating ILC1, ILC2 and ILC3 in the HD and SSc blood. (E) Correlations between circulating ILC1, ILC2 and ILC3 with the extent of cutaneous fibrosis (modified Rodnan skin thickness score (mRSS)). Data are the mean±SEM (n=59 and 73 for HDs and patients with SSc, respectively). Comparisons between groups were calculated using Mann-Whitney U test. **P<0.01; ****p<0.0001.

online supplemental figure 1AC, respectively), with ILC1, ILC2 and ILC3 being 74%, 15% and 11% in SSc and 55%, 18% and 27% in HDs, respectively (figure 1C). When focusing on ILC2 defined as Lin$^-$CD45$^+$CD127$^+$CRTH2$^+$, their frequency and absolute numbers were approximately three times lower in SSc compared with HDs (figure 1D and online supplemental figure 1BD, respectively). However, no differences in the frequency of KLRG1$^+$ ILC2 were found (online supplemental figure 1CE). Decreased were also the frequency and absolute numbers of ILC3, but not of ILC1 when SSc and HDs were compared (figure 1D and online supplemental figure 1BD).

To evaluate the clinical relevance of these observations, we analysed the ILC numbers to different relevant clinical parameters. We specifically observed a correlation between the quantity of circulating ILC2 and the modified Rodnan skin thickness score (mRSS), showing that lower is the amount of circulating ILC2 and higher is the cutaneous fibrosis (figure 1E and online supplemental figure 1DF). Of note, the ILC1 and ILC3 frequencies were not correlated with the mRSS. When comparing patients with or without interstitial lung disease, we found no difference on the % and the absolute count of ILC2 in the whole blood and there were also no differences according to the severity of interstitial lung disease or the disease duration (data not shown). Collectively, our data indicate that patients with SSc are characterised by a significant reduction in the proportion and number of circulating ILC2, which is correlated with the extent of skin fibrosis.

ILC2 are increased in human SSc skin and correlated with the extent of fibrosis

Since circulating ILCs were decreased, we further characterise ILCs infiltration in the skin. We first extracted cells from the skin and performed flow cytometry analysis. Representative staining depicting the gating strategy for ILCs and subpopulation categorisation is shown in figure 2A and online supplemental figure 2A. As suspected, we found that the percentage of total ILCs among CD45$^+$ cells was increased in the SSc skin compared with that in the HD skin (figure 2B). When evaluating the repartition of ILC subsets among the total skin ILCs, we observed that 69% were ILC2 in the HDs vs 77% in the patients with SSc, 27% were ILC1 in the HDs vs 19% in the patients with SSc (figure 2C), while ILC3 were barely detectable. When analysed among CD45$^+$ cells, a significant increase in ILC2 was observed in the SSc skin compared with the HD skin (figure 2D). The ILC1 frequency was similar in the patients with SSc and HDs (online supplemental figure 2AB), even if the proportion among ILCs was decreased in the patients with SSc compared with that in the HDs (figure 2C). The increased percentage of ILC2s among CD45$^+$ skin cells was correlated with the extent of skin fibrosis (figure 2E), whereas the ILC1 percentage did not show this correlation (online supplemental figure 2BC).

To validate this analysis and gain more insights on the precise localisation and quantification of ILC2 in the skin, we performed tissue immunofluorescence staining. Representative staining

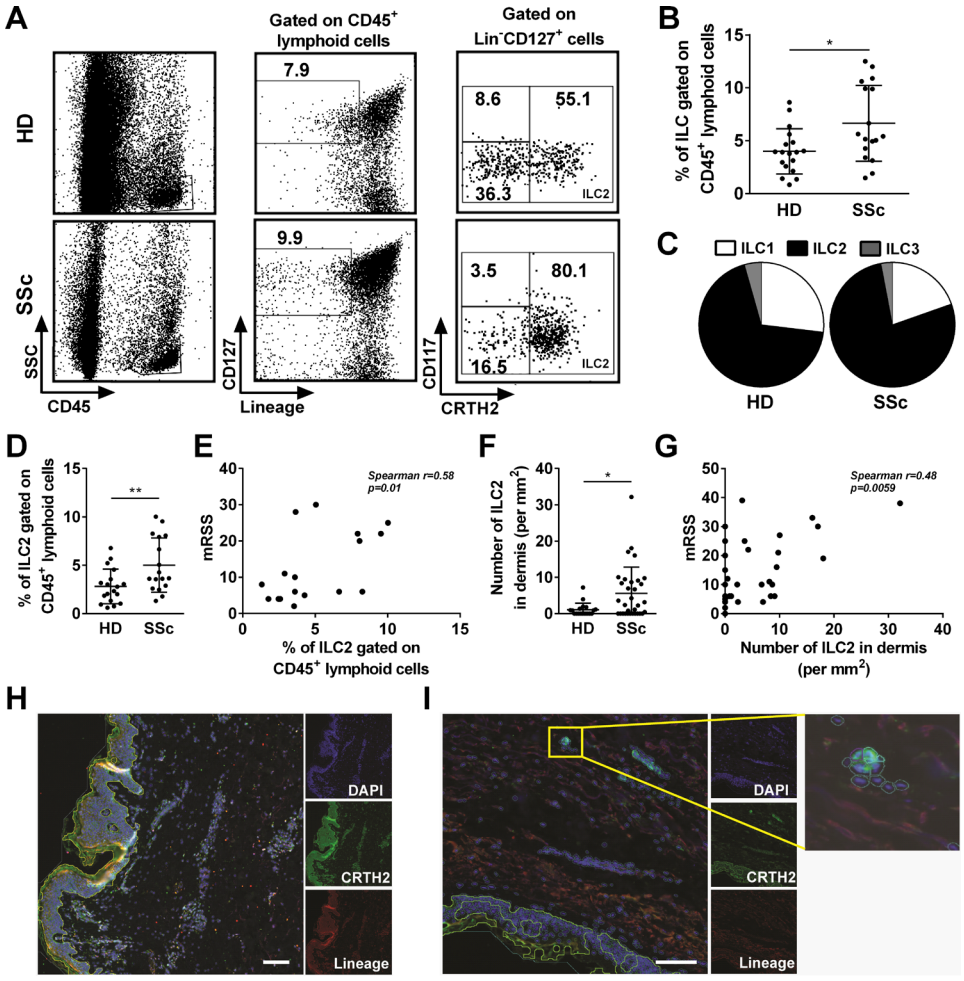

Figure 2 Characterisation of cutaneous innate lymphoid cells (ILC)-2 (ILC2) in patients with systemic sclerosis (SSc) and healthy donors (HDs). (A) Representative dot plot of cutaneous ILCs in the HD and SSc skin samples and (B) ILC frequency quantification. (C) Proportion of ILC subsets in the skin of HDs and patients with SSc. (D) Percentage of ILC2 among $CD45^+$ lymphoid cells in the HD and SSc skin samples. (E) Positive correlation between the percentage of ILC2 among $CD45^+$ cells and the extent of cutaneous fibrosis (modified Rodnan skin thickness score (mRSS)). (F) Number of ILC2 per mm^2 in the dermis of HD and SSc skin. (G) Correlation between the extent of cutaneous fibrosis (mRSS) and the number of ILC2 per mm^2 in the dermis. (H and I) Representative picture of an immunofluorescence assay using anti-CRTH2-based immunofluorescence (green) and antilineage (CD3, CD11b and FcεR1)-based immunofluorescence (red) performed to detect $CRTH2^+Lin^-$ ILC2 in the HD and SSc skin samples (scale bars=100 µm). Bar graphs show data as the mean±SEM (n=18–20 and 17–32 for HD and SSc, respectively). Comparisons between groups were calculated using Mann-Whitney U test. *P<0.05; **p<0.01.

of ILC2 ($Lin^-DAPI^+CRTH2^+$) for an HD and an SSc patient is depicted in figure 2H,I. An analysis of the ILC2 distribution and quantification revealed that the number of ILC2 per surface area (mm^2) and the percentage of ILC2 (per total cell count) were increased in the patients with SSc compared with the HDs in the dermis (figure 2F and online supplemental figure 2CD). Of interest, the number of ILC2 per mm^2 in the dermis was positively correlated with the extent of skin fibrosis as assessed by mRSS at the time of biopsy (figure 2G).

Overall, these results show that ILC2 are increased in human SSc skin and their frequency in the dermis is associated with skin fibrosis.

KLRG1 expression on skin ILC2 is modified over the course of the disease

To determine the phenotype of cutaneous ILC2 in the SSc skin, we studied the expression of several markers: HLA DR, OX40L, CCR10, CCR6, CLA, TSLPR and KLRG1 (figure 3A,B). The percentage of ILC2 expressing HLA-DR, OX40L, CCR6, CCR10, CLA and TSLPR was similar in the skin of the patients with SSc and HDs. In sharp contrast, the percentage of KLRG1-positive cells was significantly lower in the SSc skin (figure 3A,B). Interestingly, the percentage of ILC2 $KLRG1^+$ tends to decrease with the extent of cutaneous fibrosis (figure 3C).

Altogether, these results indicated that surface KLRG1 expression on ILC2 decreases in the SSc skin and may correlate with the extent of skin fibrosis thus raising the question of the functional relevance of this observation.

TGFβ promotes in vitro KLRG1 modulation of ILC2 and impacts IL10 secretion

The relevance of KLRG1 in ILC2 modulation are uncertain and remains to be proven, particularly in human SSc. To identify the factors implicated in KLRG1 modulation, we sorted ILC2 from the peripheral blood of HDs (online supplemental figure 3A) and expanded this population in vitro in the presence of IL1β and IL2 as previously described.[20] At the end of the culture, ILC2 were consistently $CD127^+CRTH2^+$ (online supplemental figure 3B) and characterised by high expression of GATA3 (online supplemental figure 3C).[21] We then tested cytokines, specifically

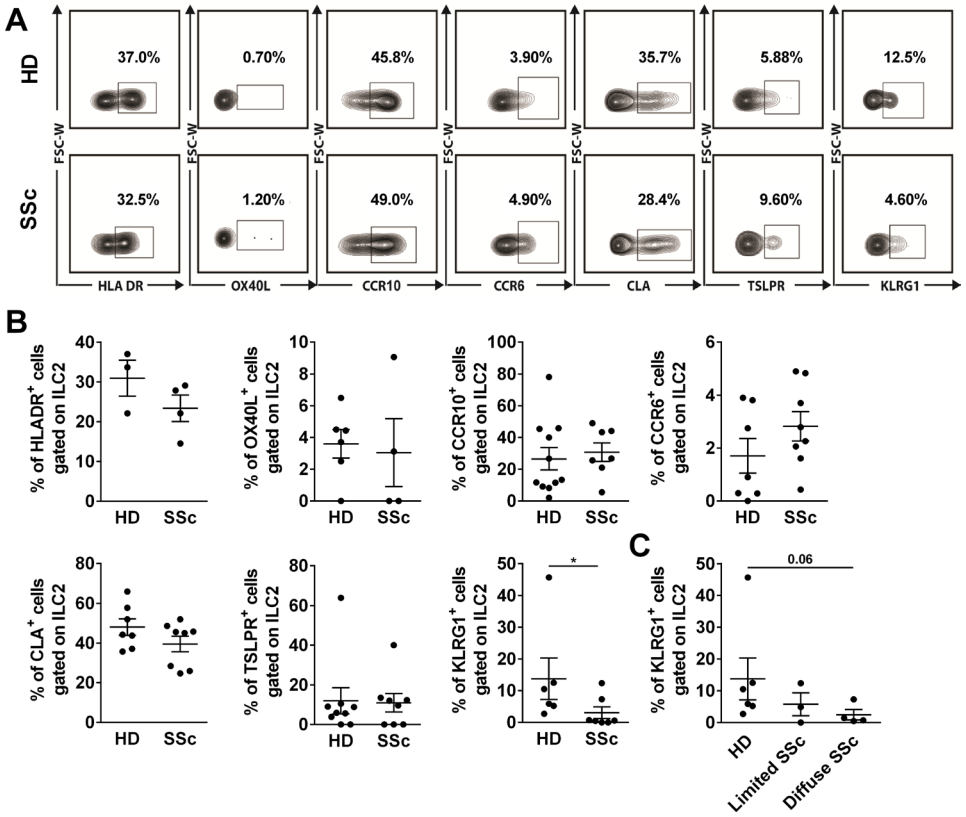

Figure 3 Decrease of killer cell lectin-like receptor G1 (KLRG1) expression on innate lymphoid cells (ILC)-2 (ILC2) in the skin of patients with systemic sclerosis (SSc). (A and B) Expression of HLA DR, OX40L, CCR10, CCR6, CLA, TSLPR and KLRG1 on skin ILC2 in the healthy donors (HDs) and patients with SSc. (C) Percentage of KLRG1$^+$ cells among ILC2s in patients with SSc with limited (Rodnan score <10) and diffuse (Rodnan score >10) in patients with SSc. Bar graphs show data as the mean±SEM (n=3–11 and 4–8 for HD and SSc, respectively). Comparisons between groups were calculated using Mann-Whitney U test. *P<0.05.

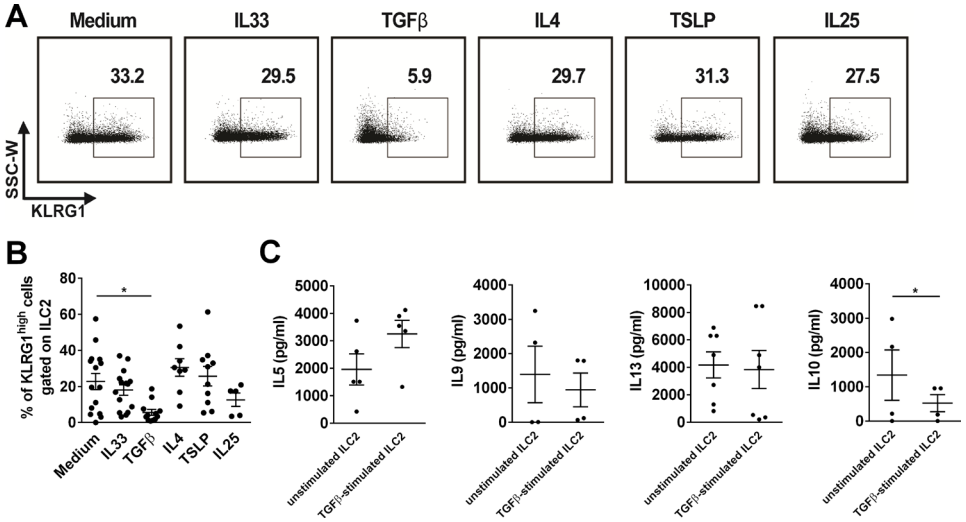

Figure 4 Transforming growth factor-β (TGFβ) affects the innate lymphoid cells (ILC)-2 (ILC2) phenotype by decreasing killer cell lectin-like receptor G1 (KLRG1) expression and interleukin (IL)10 production. (A) Representative dot blot of KLRG1 expression and (B) percentage of KLRG1$^+$ cells in unstimulated ILC2 (medium) and ILC2 stimulated with IL33, TGFβ, IL4, thymic stromal lymphopoietin (TSLP) and IL25 after 20 days of amplification. (C) Secretion of IL5, IL9, IL13 and IL10 assessed by a cytokine bead assay (CBA) in both types of ILC2 supernatants. Bar graphs show data as the mean±SEM (n=5–16 for KLRG1 expression and n=4–7 for CBA). Comparisons between groups were calculated using Kruskal-Wallis or Wilcoxon tests. *P<0.05.

involved in human SSc, for their ability to modulate KLRG1 expression on expanded ILC2. IL33, IL4, TSLP and IL25 did not modify KLRG1 expression while TGFβ dramatically decreased the expression of KLRG1 on ILC2 (figure 4A,B).

We then evaluated the functional consequences of TGFβ exposure on ILC2 by analysing its impact on cytokine production. The levels of IL5, IL9 and IL13 were similar in ILC2 exposed or not to TGFβ (figure 4C). In contrast, the production of IL10

in TGFβ-primed ILC2 was significantly reduced compared with that of controls.

Overall, these data indicate that TGFβ downregulates KLRG1 expression on ILC2, whose phenotype is associated with a decreased capability to produce IL10.

IL10 decreased production by TGFβ-stimulated ILC2 leads to a profibrotic profile by fibroblasts

Our observations suggest that the KLRG1$^-$ ILC2 population could be involved in the fibrotic process. We therefore investigated the ability of TGFβ-stimulated ILC2 to modify the fibrotic response. To this end, supernatants (SN) from TGFβ-stimulated or unstimulated ILC2 were added to dermal fibroblasts. After 1 day of co-culture, the expression of type I collagen (*COL1A1*) and matrix metalloproteinase-1 (*MMP-1*) was evaluated. As expected, TGFβ alone increased *COL1A1* and decreased *MMP1* messenger RNA (mRNA) expression (figure 5A). TGFβ neutralisation completely blocked these changes. Interestingly, SN from TGFβ-stimulated ILC2 increased the *COL1A1* mRNA expression while the SN from unstimulated ILC2 did not affect the *COL1A1* mRNA levels. Importantly, TGFβ neutralisation in TGFβ-stimulated ILC2 did not affect these results, thereby ruling out the effect of the initial exogenously added TGFβ on the induction of *COL1A1* mRNA in fibroblasts. Furthermore, ILC2 SN dramatically increased the *MMP1* mRNA expression independently of the priming conditions (figure 5A). The profibrotic activity of TGFβ-stimulated ILC2 was emphasised by the *COL1A1*/*MMP1* ratio as a surrogate of collagen turnover, which was increased, suggesting an enhanced collagen deposition over degradation (figure 5B). While no difference of expression was observed for *COL1A2*, the SN of TGFβ-stimulated ILC2 also increased the mRNA of fibronectin (figure 5C).

Since the production of IL10 was specifically reduced in TGFβ-stimulated ILC2, we next evaluated the role of IL10 on their profibrotic activity. Of interest, when IL10 was neutralised in control ILC2 SN we observed enhanced *COL1A1* mRNA expression of dermal fibroblast (figure 5D). Conversely, the addition of IL10 to TGFβ-stimulated ILC2 SN led to a dramatic decrease in *COL1A1* mRNA expression. We then confirmed these results at the protein level (figure 5E). To further explore the fibroblast activation, we measured the proliferation and the differentiation into myofibroblasts. While no difference was observed regarding the proliferation (figure 5F), we found a significant increase expression of α-smooth muscle actin when fibroblasts were incubated with the SN of TGFβ-stimulated ILC2, independently of IL10 (figure 5G). As previously, we paid attention to incubate the SN of TGFβ-stimulated ILC2 with anti-TGFβ blocking antibody, excluding the possibility that residual TGFβ from ILC2 activation may have mediated myofibroblast differentiation.

Collectively, our data show that TGFβ favours the generation of KLRG1$^-$ ILC2 characterised by low IL10 production capacity, which simultaneously results in their enhanced profibrotic capacity.

Transcriptomic analysis reveals additional fibrotic potential of TGFβ-stimulated ILC2

To look further on the fibrotic potential of human ILC2, we evaluated the transcriptome of TGFβ-stimulated ILC2 compared with unstimulated ILC2 by RNAseq (online supplemental figure 4A). The heat map shows modification in gene expression of ILC2 triggered by TGFβ activation, with 2840 genes being differentially expressed (p-adjusted value <0.01). The enrichment analysis with R library Gprofiler2 (V.0.2.0), using Gene

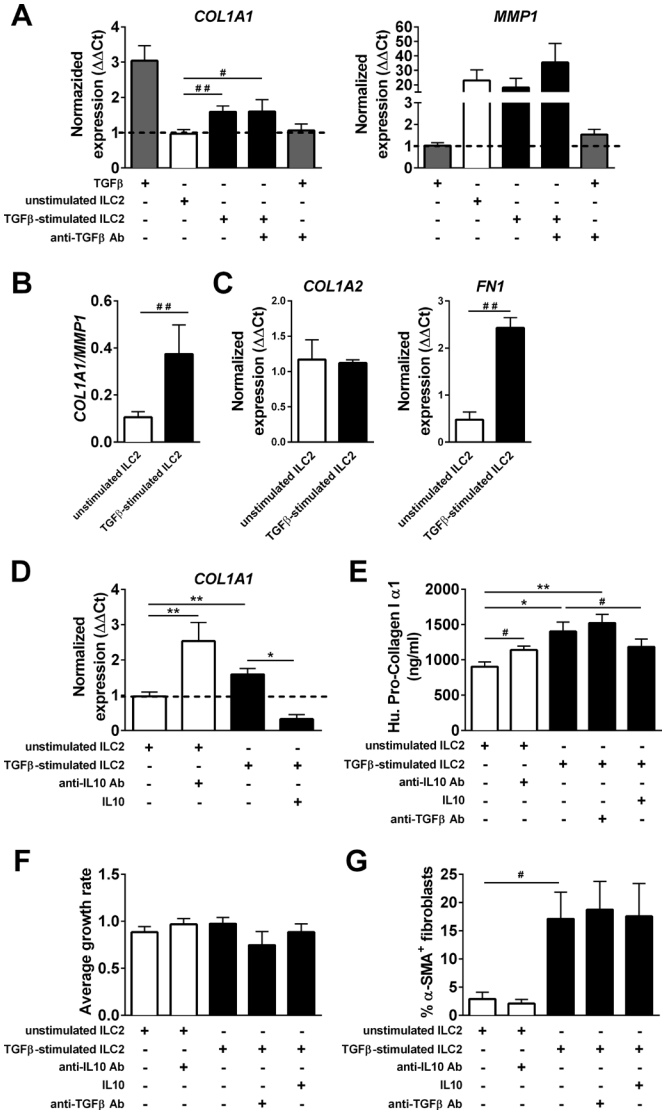

Figure 5 Transforming growth factor-β (TGFβ) exerts an indirect fibrotic role through innate lymphoid cells (ILC)-2 (ILC2) and interleukin (IL)10 secretion. (A) Q-RT-PCR analysis of type I collagen (*COL1A1*) and matrix metalloproteinase-1 (*MMP-1*) messenger RNA (mRNA) expression and (B) *COL1A1/MMP1* ratio, in fibroblasts from healthy donors (HDs), incubated with TGFβ or supernatant of unstimulated ILC2 or supernatant of TGFβ-stimulated ILC2 with or without blocking antibodies against TGFβ. (C) Q-RT-PCR analysis of *COL1A2* and *FN1* mRNA expression. (D) Q-RT-PCR analysis of *COL1A1* expression in fibroblasts incubated with supernatant of unstimulated ILC2 (in the presence or absence of anti-IL10 antibodies) and supernatant of TGFβ-stimulated ILC2 (with or without IL10). (E) Human pro-collagen I α1 concentration were analysed in the supernatants of fibroblasts from HDs after 48 hours of activation with ILC2 supernatants. (F) Average growth rate of fibroblasts were analysed after 48 hours of proliferation. (G) The percentage of α-smooth muscle actin positive fibroblasts were analysed after 72 hours of activation. Bar graphs show data as the mean±SEM (n=7–15). Comparisons between groups were calculated using the paired Wilcoxon (#) or the Kruskal-Wallis tests (*). *P<0.05; **p<0.01.

Ontology databases, indicated SMADs activation ('heteromeric SMAD protein complex'; GO:0071144; p adjusted value=4.01E^{-2} and 'SMAD protein complex'; GO:0071141; p adjusted value=4.45E^{-2}) and immune regulation (online

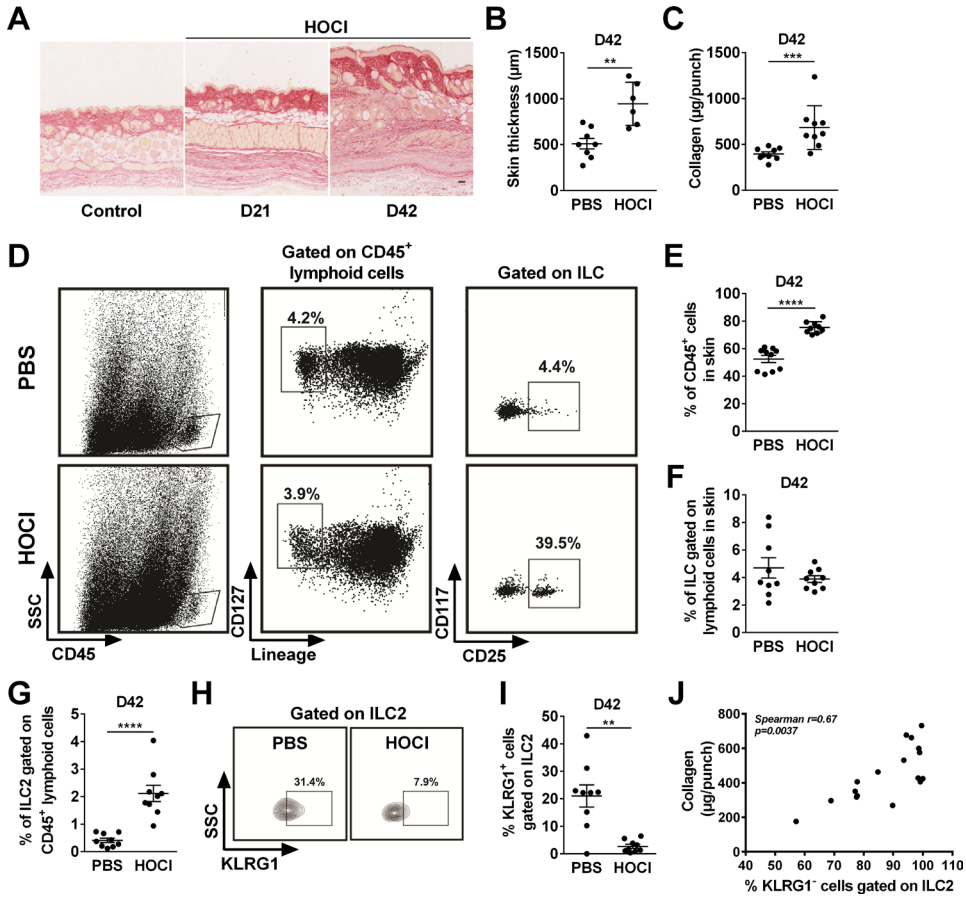

Figure 6 Characterisation of innate lymphoid cells (ILC)-2 (ILC2) in the skin of phosphate-buffered saline (PBS)-treated and hypochlorous acid (HOCl)-treated mice. (A) Picrosirius red staining of the control and systemic sclerosis (SSc) skin mice at day 42 (scale bar=10 µm). (B and C) Measure of skin thickness (µm) and collagen (µg) in the skin of PBS-treated and HOCl-treated mice at day 42. (D) Representative dot plot of cutaneous ILCs ($CD45^+$, Lin^-, $CD127^+$) and ILC2 ($CD45^+$, Lin^-, $CD127^+$, $CD25^+$) in both mice skin. (E) Percentage of $CD45^+$ cells in the skin of PBS-treated and HOCl-treated mice at day 42. (F) Percentage of ILC and (G) ILC2, among lymphoid cells in the skin of PBS-treated and HOCl-treated mice at day 42. (H and I) Percentage of $KLRG1^+$ cells among ILC2 in the skin of PBS-treated and HOCl-treated mice at day 42. (J) Positive correlation between the quantity of collagen (µg) and the percentage of $KLRG1^-$ ILC2. Bar graphs show data as the mean±SEM (n=10 per groups). Comparisons between groups were calculated using Mann-Whitney U test. **P<0.01; ***p<0.001; ****p<0.0001.

supplemental table E3, E4, E5, E6 and E7). In the first 60 most upregulated genes (online supplemental table E8), we look at genes already described in fibrosis mechanisms. Interestingly, we observed an upregulation of *LTC4S* (leukotriene C4 synthase) (log2 fold change=2.71; p adjusted value=$9.89E^{-22}$). Regarding downregulated genes, we found a decrease of *IL10* (log2 fold change=−3.71; p adjusted value=$1.36E^{-51}$), in agreement with the low IL10 expression at the protein level (figure 4C). Transcriptomic results for *IL10* and *LTC4S* were confirmed by Q-RT-PCR (online supplemental figure 4B).

$KLRG1^-$ ILC2 are enriched in the skin of hypochlorous acid-treated mice and their numbers correlate with the extent of skin fibrosis

To assess the in vivo relevance of our findings, we monitored ILC2 in the hypochlorous acid (HOCl)-induced mouse model of SSc, which recapitulates the main hallmarks of SSc.[22] At day 42, parallel to an increase in dermal thickness (figure 6A for a representative histology of the skin, figure 6B,C for skin thickness and collagen content, respectively), we observed a significant enrichment of the lymphoid cell infiltrate (figure 6D,E). Remarkably, while the frequency of ILCs was not changed (figure 6F), the frequency of ILC2 cells was more than 5 times greater in HOCl-treated skin mice compared with controls as detected by flow cytometry (figure 6G). In addition, the absolute value of cutaneous ILC2 was significantly higher in HOCl-treated mice compared with control mouse (online supplemental figure 5A). This ILC2 enrichment was specific, since the frequency and absolute count of total ILCs was not different in HOCl-treated and non-treated mice (figure 6F and online supplemental figure 5B). A slighter increase in ILC2 number and absolute count was already observed even before complete establishment of skin fibrosis (online supplemental figure 5C,D and E,F for skin thickness and collagen content, respectively). Furthermore, the frequency of KLRG1 in ILC2 was fourfold lower in HOCl-treated compared with control mice (figure 6H for a representative staining of ILC2 and figure 6I for quantification). Interestingly, we observed a strong positive correlation between the proportion of $KLRG1^-$ ILC2 and the extent of skin fibrosis (figure 6J).

The combined administration of IL10 and TGFβ inhibition is required to restore skin $KLRG1^+$ ILC2 and to prevent skin fibrosis

We have shown that the TGFβ-priming of human $KLRG1^-$ ILC2 enhances their profibrotic potential by specifically reducing their production of IL10, thus attenuating a negative feedback loop. We then addressed the question of the in vivo relevance of these findings by taking advantage of the HOCl mouse model of SSc. To inhibit TGFβ signalling, HOCl-treated mice received daily

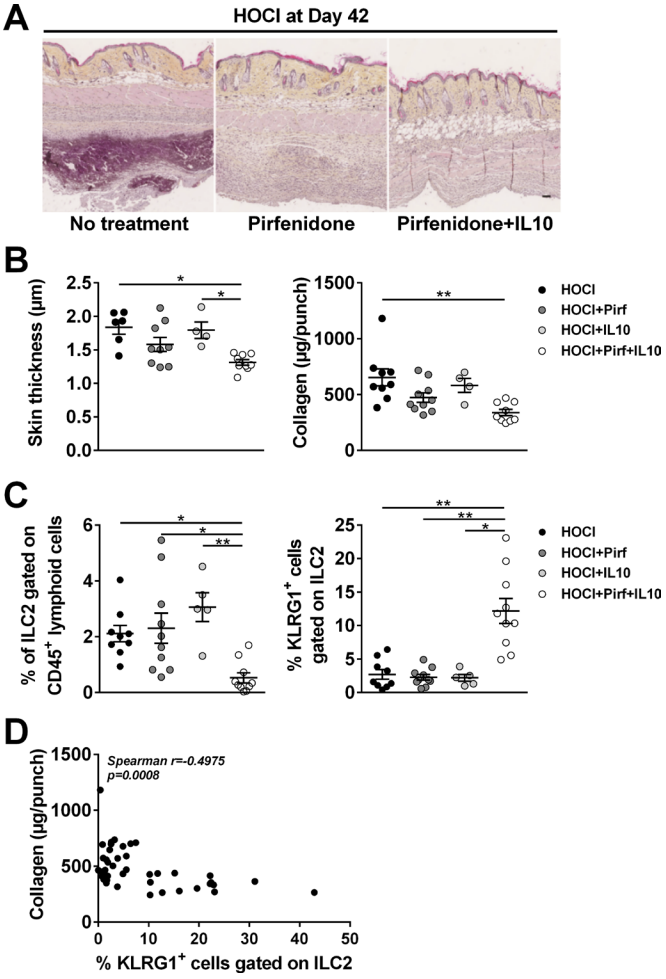

Figure 7 Interleukin (IL)10 and pirfenidone (Pirf) reduce fibrosis and affect the number of innate lymphoid cells (ILC)-2 (ILC2) in the skin of hypochlorous acid (HOCl)-treated mice at day 42. (A) H&E saffron staining of HOCl skin mice treated or untreated (scale bar=10 µm). (B) Measure of skin thickness (µm) and collagen (µg) in the skin of HOCl-untreated and HOCl-treated mice at day 42. (C) Percentage of ILC2 among lymphoid cells and percentage of KLRG1$^+$ cells among ILC2 in the skin of HOCl-untreated and HOCl-treated mice at day 42. (D) Negative correlation between collagen assay (µg) and the percentage of KLRG1$^+$ ILC2 in the skin. Bar graphs show data as the mean±SEM (n=10 per groups). Comparisons between groups were calculated using Kruskal-Wallis test. *P<0.05; **p<0.01.

oral pirfenidone for 42 days, or PBS as control. In addition, they were injected or not with daily IL10. At day 42, the treatment with pirfenidone alone moderately reduced, without reaching statistical significance, the fibrotic response assessed as skin thickness and collagen content (figure 7A,B). The treatment with IL10 by itself had no effect on skin fibrosis. In contrast, when pirfenidone and IL10 were administered jointly we observed a dramatic and statistically significant reduction in both the skin thickness and collagen content (figure 7B). Interestingly, the proportion of ILC2 was significantly lower and the frequency of their KLRG1$^+$ subset was significantly higher in HOCl mice that received the combined treatment with pirfenidone and IL10 when compared with all the other treatments (figure 7C). Not the least, the extent of collagen content in the skin was inversely correlated with the frequency of KLRG1$^+$ ILC2 (figure 7D). Altogether, these results demonstrate that the combined treatment with pirfenidone and IL10 strongly reduces skin fibrosis in vivo simultaneously reducing the number of ILC2 infiltrating the skin and enhancing their expression of KLRG1.

DISCUSSION

ILCs were recently identified as new important actors of the innate arm of the immune system. ILCs have been characterised and classified in recent years, and they have been directly implicated in many inflammatory conditions, including fibrosis, atopic dermatitis, asthma and inflammatory bowel disease.[23–26] SSc is a complex autoimmune connective tissue disease characterised by autoimmunity, widespread tissue fibrosis of the skin and internal organs and vasculopathic alterations. Its pathogenesis remains poorly understood, and a single treatment has not been approved over the last 50 years.

Our study directly implicates the impairment of ILC homeostasis as a potential contributor and new therapeutic strategy for SSc. Specifically, we observed that human skin biopsies from patients with SSc were characterised by a higher proportion of KLRG1$^-$ ILC2 positively correlated to the severity of the fibrotic process. Mechanistically, we demonstrated in vitro that TGFβ decreased KLRG1 expression on ILC2 and enhanced their profibrotic function through IL10 downregulation. Interestingly, in a mouse model of SSc recapitulating human findings, TGFβ inhibition associated with IL10 administration prevented the development of fibrosis while repopulating the skin via KLRG1$^+$ ILC2 in a synergistic manner. Altogether, those results revealed a previously undescribed mechanism in human SSc pathogenesis and paved the way for potential alternative therapeutic strategies based on TGFβ blocking associated with IL10 administration.

Few previous studies have investigated the role of ILCs in human SSc. One group described an increased number of CD4$^+$ group 1 ILCs,[27] while another group reported an increased proportion of ILC2 in the peripheral blood.[19] In contrast, our data showed a decrease in ILC2 numbers/proportions at the blood level and did not identify a difference for ILC1. We cannot exclude that immunomodulatory agents may have participated to the decrease of ILC2 in the blood. However, in the limit of the number of analysed patients, no impact on the increase amount of ILC2 in the skin of patients with SSc was observed. These contradictory observations also raised specific questions about the phenotypic definition of low-number circulating cells. Although key researchers in the field have reviewed this important question,[28] differences in gating strategies, antibodies or even methods may explain these discrepancies. In our gating strategy, one may argue that the gate for ILC is too close from the lineage positive cells. As shown in the online supplemental figure 1B, we pay attention to evaluate that the population edging the lineage positive cells also contained ILC1, ILC2 and ILC3 subsets. Regarding selected markers in our experiments, we used the CD5 in the lineage marker to remove CD4$^+$ T lymphocytes. A recent paper showed that CD5$^+$ ILCs are functionally immature and very close to progenitor cells.[29] Although CD5 could be expressed in a small proportion of ILC1, ILC2 and ILC3, these cells become functionally active cytokine-secreting ILCs when they downregulate CD5 and migrate to tissues. Therefore, using CD5 as we have done, appears to be a reasonable trade-off for eliminating CD4 T cells without losing mature cells. Finally, by using two complementary strategies, we observed an increase in the proportion of ILC2 in the SSc skin in accordance with a previously published report.[19]

Extensive characterisation of human skin-homing ILC2 from patients with SSc revealed subtle phenotypic changes associated with the fibrotic process. SSc skin is populated by

KLRG1$^-$ ILC2, whereas skin-resident ILC2 express KLRG1 in normal skin from humans and mice. Interestingly, KLRG1 expression levels have been described as a marker to separate iILC2 (KLRG1$^+$) and nILC2 (KLRG1$^-$). iILC2 could be transient progenitors and develop into nILC2 or ILC3-like cells.[30] Although this dichotomy has mainly been described in the field of infection in mice, our results show that this observation is true in humans and would be directly associated with the fibrotic process. Our results in SSc suggest KLRG1$^+$ ILC2 could migrate from the blood to the skin and switch into profibrotic KLRG1$^-$ ILC2. Functional studies in vitro revealed that TGFβ, which is known to be elevated in patients with SSc, was a key cytokine involved in KLRG1 downregulation, thus mirroring the effect of TGFb on KLRG1-expressing CD8$^+$ T cells.[31] Unexpectedly, we observed that KLRG1$^-$ ILC2 triggered profibrotic responses on dermal fibroblast, which was mainly due to an imbalance in production between profibrotic factors and antifibrotic factors. Moreover, we observed that the low capability to secrete IL10 was directly responsible for the profibrotic effect. The role of IL10 as an antifibrotic agent has been previously demonstrated. Indeed, two distinct models of fibrosis, one in chronic renal insufficiency and another in hepatic damage induced by biliary duct ligation, provide evidence for the impact of decreased levels of IL10 in the occurrence and maintenance of fibrosis.[32 33] Moreover, the genetic delivery of IL10 significantly attenuated TGFβ production in the lungs of mice subjected to bleomycin-induced pulmonary fibrosis. This effect was still observed when IL10 was delivered at later time points when fibrosis was already established.[34] Therefore, our results established a direct link between TGFβ and low secretion of IL10 at the tissue level through ILC2.

To look further on the fibrotic potential of ILC2, we evaluated the transcriptome of TGFβ-stimulated ILC2 compared with unstimulated ILC2 and found an increase of the leukotriene C4 synthase expression, suggesting that activated ILC2 may release leukotriene C4 (LTC4). Since LTC4 is a potent inducer of collagen synthesis by dermal fibroblasts,[35] the ILC2-LTC4 axis in SSc skin fibrosis will require further investigations.

Different SSc mice models have been used to evaluate different therapeutic strategies; however, none of them recapitulates the human observations *in integro*. The HOCl-treated mouse model has the advantage of summarising the three main characteristics of SSc: vasculopathy, deregulation of the immune response (including the production of autoantibodies) and cutaneous and pulmonary fibrosis. In our study, we only tested our hypothesis in one mouse model that constitutes a limitation. However, our data indicated that this model recapitulated the human skin findings, including the increased proportion of KLRG1$^-$ skin ILC2 proportions correlated to the fibrotic process. We were not able to increase lung fibrosis, precluding any further pulmonary investigation. Our work is thus limited to only one mouse model exploring cutaneous fibrosis. Many mouse models potentially useful to further assess the relevance of ILC in experimental animals could be considered, of which none fully recapitulates the features of human systemic sclerosis.[36] However, we believe that, within its limits, the HOCl mouse model we adopted, strongly support the results of our research principally and extensively made in humans. In detail, it met several important requirements for our demonstration: (i) development of skin fibrosis after an inflammatory period; (ii) accompanied by an increase of ILC2 in the skin; (iii) a positive correlation between skin fibrosis and number of ILC2 in the skin, as we have shown in humans. From a therapeutic perspective, most of the mouse models have implicated ILC2 through its deletion using *Rora*$^{sg/flox}$*Il7r*$^{Cre/+}$ mice[37] or *Rag1*$^{-/-}$ mice, for instance, coupled with the injection of depleting anti-Thy1 antibody.[38] Although these strategies offer a clear view of the global implication of ILC2 in a model, it is not a feasible strategy in humans and does not permit the characterisation of the implication of ILC2-skewed functionalities in a disease process, as it is the case in our setting. Therefore, we decided to adopt an alternative strategy that combines a well-accepted TGFβ inhibitor and IL10 supplementation, according to our in vitro data. Our results revealed a dramatic synergic effect on the fibrotic process while KLGR1$^+$ ILC2 were repopulating the skin. Although this therapeutic strategy does not formally directly prove the involvement of the KLRG1$^-$ population in the pathogenesis, it provides indirect evidence on the pathogenic loop implicating ILC2, IL10 and TGFβ. Moreover, our results could constitute the groundwork for proposing a clinical trial testing the combination of the TGFβ inhibitor and IL10 in patients with SSc. The US Food and Drug Administration recently approved targeting the TGFβ pathway for the treatment of idiopathic pulmonary fibrosis (IPF). In a phase III clinical trial, pirfenidone successfully reduced the progression of IPF and was associated with fewer deaths.[39] For unknown reasons, this effect in the patients with SSc seemed to be milder; thus, combining another strategy in this multifactorial disease could be an option. After the successful preclinical experiments, clinical studies using human recombinant IL10 are already in progress for the treatment of inflammatory bowel diseases with an acceptable safety profile.[40] Future studies using nintedanib instead of pirfenidone are also of interest since this molecule is used in interstitial lung disease in SSc.[41]

In conclusion, our study revealed that ILC2 may contribute to the fibrotic process observed in human SSc and the combination of the TGFβ inhibitor and IL10 could be a promising therapeutic strategy.

Author affiliations
[1]ImmunoConcEpt, CNRS, UMR 5164, University of Bordeaux, Talence, France
[2]Rheumatology Department, CHU de Bordeaux, Bordeaux, France
[3]Immunology Department, CHU Cochin Hospital, University of Paris Descartes Faculty of Medicine Paris Center, Paris, France
[4]Animal Facility A2, University of Bordeaux, Talence, France
[5]Centre de Bioinformatique de Bordeaux (CBiB), University of Bordeaux, Talence, France
[6]IBGC, CNRS, UMR 5095, University of Bordeaux, Talence, France
[7]Dermatology Department, CHU de Bordeaux, Bordeaux, France
[8]INSERM U1035, University of Bordeaux, Talence, France
[9]Vascular Medicine Department, CHU de Bordeaux, Bordeaux, France
[10]Immunology and Allergy, University of Geneva, Geneva, Switzerland
[11]Internal Medicine, CHU de Bordeaux, Bordeaux, France
[12]Hematology, CHU de Bordeaux, Bordeaux, France
[13]Immunology department, CHU de Bordeaux, Bordeaux, France

Acknowledgements Some of the data were presented in an abstract at the EULAR annual meeting in 2016. Victor Racine and the QuantaCell society are acknowledged for their help with the analysis of the human imaging data. The histological studies were performed at the Experimental Histopathology Platform, INSERM US 005-CNRS UMS 3427-TBM CORE, a service unit of the CNRS-INSERM and Bordeaux University. The help of Nathalie Dugot-Senant is acknowledged. The microscopy analyses were performed at the Bordeaux Imaging Centre, a service unit of the CNRS-INSERM and Bordeaux University, member of the national infrastructure France BioImaging supported by the French National Research Agency (ANR-10-INBS-04). The help of Sébastien Marais is acknowledged. We are also grateful to Atika Zouine and Vincent Pitard for their expert assistance in flow cytometry (Plateforme de Cytométrie en Flux, SFR TransBioMed, Université Bordeaux), Xavier Gauthereau for assistance in PCR (Plateforme de Q-PCR SFR TransBioMed, Université Bordeaux) and Benoit Rousseau for help in the animal facility (Animalerie A2, Université Bordeaux). RNAseq experiment were realised with the genom'IC platform (INSERM U1016, Institut Cochin). Part of the computational resources and infrastructure used in present publication were provided by the Bordeaux Bioinformatics Centre (CBiB). Eric Vivier and Frédéric Vély are acknowledged for helping us in the setting of ILC staining. Andreas Ramming and Jörg Distler are acknowledged for providing stimulating discussions on the data.

Collaborators Victor Racine, Nathalie Dugot-Senant, Sébastien Marais, Atika Zouine, Vincent Pitard, Xavier Gauthereau, Benoit Rousseau, Eric Vivier, Frédéric Vély, Andreas Ramming, Jörg Distler.

Contributors PL and BA jointly designed the research, performed the experiments, collected, analysed and interpreted the data, wrote and revised the manuscript. MJ, PM, EL, DL, AG and VJ performed and analysed some experiments. EL, PL, JI, MJ and FB performed mice experiments. TS, CC, TP and PB provided intellectual input and edited the manuscript. PM, DL, PH, JS, JC, CR, PD, TS, EL and EF recruited the study participants and provided patients' samples and clinical data. CC-B and M-ET jointly designed and supervised the study and wrote the manuscript.

Funding This research was supported by grants from the Société Française de Rhumatologie (SFR), Rhumato-Network. It was also supported by the Association des Sclérodermiques de France (ASF).

Competing interests None declared.

Patient consent for publication Not required.

Ethics approval Ethical approval information: human participants: Patients were included in the context of the VISS (Vasculopathy and Inflammation in Systemic Sclerosis) biomedical research project founded in 2012 and approved by the institutional ethical committee (CPP, 2012-A00081-42, Aquitaine). All participants provided written informed consent before inclusion. Ethical approval information: animals: Comité d'éthique pour l'expérimentation animale de Bordeaux (CE50) (project n°15544).

Provenance and peer review Not commissioned; externally peer reviewed.

Data availability statement Data are available on reasonable request.

ORCID iDs
Benoit Allard http://orcid.org/0000-0002-7093-5851
Damien Leleu http://orcid.org/0000-0003-3265-3201
Carlo Chizzolini http://orcid.org/0000-0003-4849-6335
Christophe Richez http://orcid.org/0000-0002-3029-8739
Cécile Contin-Bordes http://orcid.org/0000-0003-4652-2907
Marie-Elise Truchetet http://orcid.org/0000-0001-8045-0180

REFERENCES

1 Denton CP, Khanna D. Systemic sclerosis. *Lancet* 2017;390:1685–99.
2 Chizzolini C, Brembilla NC, Montanari E, *et al*. Fibrosis and immune dysregulation in systemic sclerosis. *Autoimmun Rev* 2011;10:276–81.
3 Laurent P, Sisirak V, Lazaro E, *et al*. Innate immunity in systemic sclerosis fibrosis: recent advances. *Front Immunol* 2018;9:9.
4 Mahoney JM, Taroni J, Martyanov V, *et al*. Systems level analysis of systemic sclerosis shows a network of immune and profibrotic pathways connected with genetic polymorphisms. *PLoS Comput Biol* 2015;11:e1004005.
5 Klose CSN, Artis D. Innate lymphoid cells as regulators of immunity, inflammation and tissue homeostasis. *Nat Immunol* 2016;17:765–74.
6 Spits H, Artis D, Colonna M, *et al*. Innate lymphoid cells--a proposal for uniform nomenclature. *Nat Rev Immunol* 2013;13:145–9.
7 Constantinides MG, McDonald BD, Verhoef PA, *et al*. A committed precursor to innate lymphoid cells. *Nature* 2014;508:397–401.
8 Jia Y, Fang X, Zhu X, *et al*. IL-13 $^{+}$ Type 2 Innate Lymphoid Cells Correlate with Asthma Control Status and Treatment Response. *Am J Respir Cell Mol Biol* 2016;55:675–83.
9 Smith SG, Chen R, Kjarsgaard M, *et al*. Increased numbers of activated group 2 innate lymphoid cells in the airways of patients with severe asthma and persistent airway eosinophilia. *J Allergy Clin Immunol* 2016;137:75–86.
10 Meng X-M, Nikolic-Paterson DJ, Lan HY. TGF-β: the master regulator of fibrosis. *Nat Rev Nephrol* 2016;12:325–38.
11 Lafyatis R. Transforming growth factor β--at the centre of systemic sclerosis. *Nat Rev Rheumatol* 2014;10:706–19.
12 Varga J, Whitfield ML. Transforming growth factor-beta in systemic sclerosis (scleroderma). *Front Biosci* 2009;1:226–35.
13 Wang L, Tang J, Yang X, *et al*. TGF-β induces ST2 and programs ILC2 development. *Nat Commun* 2020;11:1–15.
14 Huang Y, Guo L, Qiu J, *et al*. IL-25-responsive, lineage-negative KLRG1(hi) cells are multipotential 'inflammatory' type 2 innate lymphoid cells. *Nat Immunol* 2015;16:161–9.
15 Huang Y, Mao K, Chen X, *et al*. S1P-dependent interorgan trafficking of group 2 innate lymphoid cells supports host defense. *Science* 2018;359:114–9.
16 Lonati PA, Brembilla NC, Montanari E, *et al*. High IL-17E and low IL-17C dermal expression identifies a fibrosis-specific motif common to morphea and systemic sclerosis. *PLoS One* 2014;9:e105008.
17 Manetti M, Guiducci S, Ceccarelli C, *et al*. Increased circulating levels of interleukin 33 in systemic sclerosis correlate with early disease stage and microvascular involvement. *Ann Rheum Dis* 2011;70:1876–8.
18 Truchetet M-E, Demoures B, Eduardo Guimaraes J, *et al*. Platelets induce thymic stromal lymphopoietin production by endothelial cells: contribution to fibrosis in human systemic sclerosis. *Arthritis Rheumatol* 2016;68:2784–94.
19 Wohlfahrt T, Usherenko S, Englbrecht M, *et al*. Type 2 innate lymphoid cell counts are increased in patients with systemic sclerosis and correlate with the extent of fibrosis. *Ann Rheum Dis* 2016;75:623–6.
20 Ohne Y, Silver JS, Thompson-Snipes L, *et al*. Il-1 is a critical regulator of group 2 innate lymphoid cell function and plasticity. *Nat Immunol* 2016;17:646–55.
21 Yagi R, Zhong C, Northrup DL, *et al*. The transcription factor GATA3 is critical for the development of all IL-7Rα-expressing innate lymphoid cells. *Immunity* 2014;40:378–88.
22 Servettaz A, Goulvestre C, Kavian N, *et al*. Selective oxidation of DNA topoisomerase 1 induces systemic sclerosis in the mouse. *J Immunol* 2009;182:5855–64.
23 Geremia A, Arancibia-Cárcamo CV, Fleming MPP, *et al*. IL-23-responsive innate lymphoid cells are increased in inflammatory bowel disease. *J Exp Med* 2011;208:1127–33.
24 Hams E, Armstrong ME, Barlow JL, *et al*. Il-25 and type 2 innate lymphoid cells induce pulmonary fibrosis. *Proc Natl Acad Sci U S A* 2014;111:367–72.
25 Jia Y, Fang X, Zhu X, *et al*. IL-13^{+} Type 2 Innate Lymphoid Cells Correlate with Asthma Control Status and Treatment Response. *Am J Respir Cell Mol Biol* 2016;55:675–83.
26 Salimi M, Barlow JL, Saunders SP, *et al*. A role for IL-25 and IL-33-driven type-2 innate lymphoid cells in atopic dermatitis. *J Exp Med* 2013;210:2939–50.
27 Roan F, Stoklasek TA, Whalen E, *et al*. Cd4+ group 1 innate lymphoid cells (ILC) form a functionally distinct ILC subset that is increased in systemic sclerosis. *J Immunol* 2016;196:2051–62.
28 Vallentin B, Barlogis V, Piperoglou C, *et al*. Innate lymphoid cells in cancer. *Cancer Immunol Res* 2015;3:1109–14.
29 Nagasawa M, Germar K, Blom B, *et al*. Human CD5^{+} Innate Lymphoid Cells Are Functionally Immature and Their Development from CD34^{+} Progenitor Cells Is Regulated by Id2. *Front Immunol* 2017;8:1047.
30 Huang Y, Paul WE. Inflammatory group 2 innate lymphoid cells. *Int Immunol* 2016;28:23–8.
31 Schwartzkopff S, Woyciechowski S, Aichele U, *et al*. TGF-β downregulates KLRG1 expression in mouse and human CD8(+) T cells. *Eur J Immunol* 2015;45:2212–7.
32 Mu W, Ouyang X, Agarwal A, *et al*. Il-10 suppresses chemokines, inflammation, and fibrosis in a model of chronic renal disease. *J Am Soc Nephrol* 2005;16:3651–60.
33 Sharawy MH, Abdel-Rahman N, Megahed N, *et al*. Paclitaxel alleviates liver fibrosis induced by bile duct ligation in rats: role of TGF-β1, IL-10 and c-myc. *Life Sci* 2018;211:245–51.
34 Nakagome K, Dohi M, Okunishi K, *et al*. In vivo IL-10 gene delivery attenuates bleomycin induced pulmonary fibrosis by inhibiting the production and activation of TGF-beta in the lung. *Thorax* 2006;61:886–94.
35 Oyoshi MK, He R, Kanaoka Y, *et al*. Eosinophil-derived leukotriene C4 signals via type 2 cysteinyl leukotriene receptor to promote skin fibrosis in a mouse model of atopic dermatitis. *Proc Natl Acad Sci U S A* 2012;109:4992–7.
36 Marangoni RG, Varga J, Tourtellotte WG. Animal models of scleroderma: recent progress. *Curr Opin Rheumatol* 2016;28:561–70.
37 Oliphant CJ, Hwang YY, Walker JA, *et al*. MHCII-mediated dialog between group 2 innate lymphoid cells and CD4(+) T cells potentiates type 2 immunity and promotes parasitic helminth expulsion. *Immunity* 2014;41:283–95.
38 Monticelli LA, Sonnenberg GF, Abt MC, *et al*. Innate lymphoid cells promote lung-tissue homeostasis after infection with influenza virus. *Nat Immunol* 2011;12:1045–54.
39 Azuma A, Taguchi Y, Ogura T, *et al*. Exploratory analysis of a phase III trial of pirfenidone identifies a subpopulation of patients with idiopathic pulmonary fibrosis as benefiting from treatment. *Respir Res* 2011;12:143.
40 Fedorak RN, Gangl A, Elson CO, *et al*. Recombinant human interleukin 10 in the treatment of patients with mild to moderately active Crohn's disease. the interleukin 10 inflammatory bowel disease Cooperative Study Group. *Gastroenterology* 2000;119:1473–82.
41 Seibold JR, Maher TM, Highland KB, *et al*. Safety and tolerability of nintedanib in patients with systemic sclerosis-associated interstitial lung disease: data from the SENSCIS trial. *Ann Rheum Dis* 2020;79:1478–84.

SUPPLEMENTAL MATERIAL

Title: TGFβ promotes low IL10-producing ILC2 with pro-fibrotic ability involved in skin fibrosis in systemic sclerosis.

Paôline Laurent[1#], Benoit Allard[1#], Pauline Manicki[2], Valérie Jolivel[1], Emeline Levionnois[1], Mohamed Jeljeli[3], Pauline Henrot[2], Julien Izotte[4], Damien Leleu[1], Alexis Groppi[5,6], Julien Seneschal[7], Joël Constans[8], Carlo Chizzolini[9], Christophe Richez[1,2], Pierre Duffau[1,10], Estibaliz Lazaro[1,10], Edouard Forcade[1,11], Thierry Schaeverbeke[1,2], Thomas Pradeu[1], Frédéric Batteux[3], Patrick Blanco[1,12], Cécile Contin-Bordes[1,12*], Marie Elise Truchetet[1,2*]

[1]ImmunoConcEpt, CNRS, UMR 5164, University of Bordeaux, France
[2]Rheumatology Department, CHU Bordeaux Hospital, Bordeaux, France
[3]Immunology Department, CHU Cochin Hospital, Université Paris Descartes, Paris, France
[4]Animal Facility A2, University of Bordeaux, France
[5]Centre de Bioinformatique de Bordeaux (CBiB), University of Bordeaux, France
[6]IBGC, CNRS, UMR 5095, University of Bordeaux, France
[7]Dermatology Department, CHU Bordeaux Hospital, Bordeaux, France
[8]Vascular Medicine Department, CHU Bordeaux Hospital, Bordeaux, France
[9]Immunology and Allergy, University Hospital and School of Medicine, Geneva, Switzerland
[10]Internal Medicine Department, CHU Bordeaux Hospital, Bordeaux, France
[11]Hemology Department, CHU Bordeaux Hospital, Bordeaux, France
[12]Immunology Department, CHU Bordeaux Hospital, Bordeaux, France

Co-first authors
* Equal contributors

Corresponding author: Marie-Elise Truchetet, CNRS UMR 5164 ImmunoConcEpt, Université de Bordeaux, 146 rue Leo Saignat, 33076 Bordeaux, France
Phone: +33 5 57 57 92 46 Fax: +33 5 57 57 14 72 ORCID: 0000-0001-8045-0180; Email: marie-elise.truchetet@chu-bordeaux.fr

The authors have declared no conflict of interest.

Funding: This research was supported by grants from the Société Française de Rhumatologie (SFR), Rhumato-Network. It was also supported by the Association des Sclérodermiques de France (ASF).

METHODS

Study population

Patients were included in the context of the VISS (Vasculopathy and Inflammation in Systemic Sclerosis) biomedical research project founded in 2012 and approved by the institutional ethical committee (CPP, 2012-A00081-42, Aquitaine). All participants provided written informed consent before inclusion. All patients satisfied the classification criteria proposed by the American College of Rheumatology (ACR) and the European League Against Rheumatism (EULAR) 2013[1]. Punch biopsy specimens (3-4 mm) of affected mid forearm skin were obtained for some patients. Clinical features are described in Table 1.

Clinical features in the study population

Age- and sex-matched healthy donors (HDs) were recruited at the local Blood Transfusion Centre (University Hospital, Bordeaux) for blood tests. For the control skin samples, biopsy specimens were isolated from skin that had been discarded during plastic surgery (brachioplasty). None of the HDs had dermatological disorders or treatment with immunosuppressant agents and/or glucocorticoids. For each patient, a disease- and organ-specific questionnaire was completed by the clinician in charge of the patient and then centralized by investigators. Clinical features (scleroderma form, sex, age at Raynaud's phenomenon (RP) onset, age at onset of the first non-RP manifestation, disease duration, and symptoms of skin, articular, heart, lung, kidney, and gastrointestinal involvement), immunologic test results (antinuclear antibodies, anti-Scl70 antibodies, and anticentromere antibodies), imaging and functional exams (thorax CT scans, respiratory function tests, cardiac ultrasonography and right heart catheterization) and treatments were recorded. For the modified Rodnan skin thickness score (mRSS) and Right Ventricle Systolic Pressure, the

highest values from the medical history were registered for each patient. Interstitial lung disease was diagnosed when pulmonary function tests showed a restrictive defect with decreased diffusion capacity (DLCO) associated with several types of lesions on thorax CT scans. Lung fibrosis was diagnosed based on specific lesions observed on thorax CT scans, i.e., honeycomb cysts and reticular septal thickening.

Animal model

Six-week-old female BALB/c mice were purchased from Janvier Laboratory (Le Genest Saint Isle, France). Animals received human care in compliance with the European Union guidelines (European Directive 2010/63/UE) and approved by the local ethics committee: *Comité d'éthique pour l'expérimentation animale de Bordeaux* (CE50) [project n°15544]. All mice were housed in ventilated cages with sterile food and water provided *ad libitum*.

Mice were randomly distributed into experimental and control groups (10 mice/group). SSc was induced according to the protocol described by Kavian *et al.*[2]. A total of 300 µl of HOCl solution was prepared extemporaneously by adding NaClO solution (9.6% active chlorine) to 100 mM of KH_2PO_4 (pH 6.2) and injected intradermally into the shaved backs of the mice (one injection of 150 µl on either side of the tail) using a 27-gauge needle every day for 6 weeks (HOCl-mice). Control mice received injections of 300 µl of sterilized PBS (PBS-mice). The mice were sacrificed at weeks 6 (apex of the fibrotic phase). Fibrosis was assessed by dermal thickness, histopathological analysis and measurement of the hydroxyproline content in the skin[2]. Among the SSc-induced mice, one group received a daily flank injection of recombinant IL10 (500ng/ml, Miltenyi Biotec), one group received daily pirfenidone gavage (300mg/kg, Roche), and one group received both treatments daily.

Isolation of ILC

In human experiments, blood samples (5 mL) were incubated with red blood cell lysis buffer (Miltenyi Biotec) for 10 min at room temperature before staining. Skin biopsies from Systemic Sclerosis (SSc) patients and healthy donors were digested with collagenase (5 mg/ml, Roche) and liberase (40 μg/mL, Roche) in HBSS at 37°C for 3 hours in a shaker and filtered through a 0.70-μm nylon mesh.

ILCs were defined as $CD45^+Lin^-CD127^+$ cells. A cocktail of antibodies against CD3, CD5, CD11c, CD14, CD16, CD19, CD31, CD34, CD56, CD94, CD123, CD303, TCR-αβ-γδ, αSMA and FcεR1 defined lineage. ILC1 were defined as $CD45^+Lin^-CD127^+CD117^-CRTH2^-$ cells; ILC2 were defined as $CD45^+Lin^-CD127^+CRTH2^+$ cells; and ILC3 were defined as $CD45^+Lin^-CD127^+CD117^+CRTH2^-$ cells[3]. All the gates were setup using Fluorescence Minus One controls and were then copied/pasted for analysis of the data on FlowJo software.

In the mouse experiments, cell suspensions from collected skin was taken from the back region of mice with a 6-mm-diameter punch (3 punches per mouse). Then, 1 ml of Dulbecco's modified Eagle's medium (DMEM) containing 1% nonessential amino acids, 1% L-glutamine, 1% sodium pyruvate, 50 units/ml penicillin, 50 mg/ml streptomycin, and 10% fetal calf serum (cDMEM, GIBCO) was added to each well of 6-well plates, and a mixture of collagenase (12.5 mg/mL, Roche) and liberase (100 μg/mL, Roche) was added to each well. After digestion for 5 hours at 37°C, the remaining tissue was passed through a 70-μm strainer (VWR) and washed with cDMEM. After centrifugation, the pellet was suspended in cold DMEM and passed through a 40-μm strainer. Cells were first gated for small/non-granular (FSC^{low}/SSC^{low}) and live (viability fixable dye positive) leukocytes ($CD45^+$). ILC2s were identified as Lin^-, $CD127^+$ and CD25 $(IL2\text{-}R\alpha)^+$.

ILC2 were quantified as the percentage of cells with lymphoid morphology $CD45^+$ Lin^- and $CRTH2^+$ cells. Absolute values of ILC2 (for blood) were calculated as the % of ILC2 *

absolute lymphocyte count (G/L) / 100. Cells were analyzed using a Fortessa flow cytometer with FACSDiva (BD), and the data analysis was performed with FlowJo 10.1.

Purification, expansion and activation of ILC2

Peripheral blood mononuclear cells (PBMCs) were isolated from HD blood (buffy coat concentrate) by Ficoll. After NK enrichment (NK cell isolation kit, Miltenyi Biotec), ILC2 were sorted using ARIA FACS (BD). Once purified, the cells were cultured in NK MACS medium (Miltenyi) with 50 units/ml penicillin, 50 mg/ml streptomycin, and 5% human serum in a 96-well round-bottom plate, with 200µl of medium/well, in the presence of IL1β (R&D Systems) and IL2 (Miltenyi Biotec), both at a concentration of 10 ng/ml, as previously described[4]. The cells were duplicated every couple of days by dividing one well in two wells and adding 100µl of fresh medium with cytokines. The ILC2 were expanded for approximately 20 days and the purity was evaluated by cytofluorimetric analysis. This phenotype demonstrated a purity > 95% of viable ILC2 cells (online supplemental figure 3B). Then, ILC2 were harvested, and extensively washed. 50 000 ILC2 were activated for 48 hours with either IL33 (Miltenyi Biotec), TGFβ (R&D Systems), IL4 (Miltenyi Biotec), TSLP (R&D Systems) or IL25 (Miltenyi Biotec). All these cytokines were used at 10 ng/ml, in NK MACS medium complemented with 5% human serum and IL2 at 10ng/ml. The 48-hour supernatants (SNs) were harvested while the cells were used for cytofluorimetric analysis.

Extraction and incubation of fibroblasts

Fibroblasts were obtained from skin biopsy samples from HDs[5]. Briefly, skin biopsy specimens were digested with 0.1% type IA collagenase at 37°C for 2 hours. Adherent cells were grown in cDMEM. Fibroblasts were used between the third and sixth passages. Then, 3.10^4 fibroblasts were cultured in duplicate in a 96-well flat-bottom plate and incubated with

non-stimulated ILC2 SNs or TGFβ-stimulated ILC2 SNs for 24 hours (50% SNs; 50% cDMEM). TGFβ (10 ng/ml) was used as a positive control. rIL10 (10 ng/ml) was added to the TGFβ-stimulated ILC2 SNs and then incubated with fibroblasts. Blocking IL10 antibody (Miltenyi Biotec, 10 ng/ml) was incubated with non-stimulated ILC2 SNs and then added to the fibroblasts. Blocking TGFβ antibody (R&D Systems, 10 ng/ml) was incubated with TGFβ-stimulated ILC2 SNs and then added to the fibroblasts. After 24 hours, the SNs were harvested and placed at -80°C, and the fibroblasts were collected with a lysis buffer.

Tissue processing and immunofluorescence

All samples were fixed in 3.8% formalin, dehydrated with graded concentrations of alcohol and finally embedded in paraffin, as described previously[6]. The tissue blocks were cut into 3-µm thin sections with a microtome (Leica RM2255). Sections were floated in a 37°C water bath, mounted on electrostatically charged adhesion slides (SuperFrost Plus, Thermo Scientific) and dried on a heating plate for 2 hours at 56°C. Sections were dewaxed with xylene and rehydrated in decreasing concentrations of ethanol. Using a PT link instrument (Dako), a heat-induced antigen retrieval (HIER) step was performed by immersion of the samples into a citrate buffer at pH 6 (PT Module Buffer 1, Thermo Scientific) for 20 min at 97°C. Then, in a humidified incubation box, the sections were saturated with a blocking buffer (PBS 10 mM pH 7.4, 0.1% Triton X-100, 5% Normal Goat Serum (Thermo Scientific)) for 1 hour at room temperature. The sections were subsequently incubated overnight at 4°C with the following antibodies diluted in blocking buffer: rabbit anti-human CRTH2 (GPR44, Novus Biologicals), mouse anti-human CD3 (PS1, Abcam), mouse anti-human CD11b (CL1719, Novus Biologicals), and mouse anti-human FcER1 (9E1, Thermo Fisher). Negative controls were systematically obtained by omitting the primary antibodies. After washing thoroughly with PBS, secondary antibodies coupled to fluorescent dyes (goat anti-rabbit

AF488, Invitrogen and goat anti-mouse AF568, Invitrogen) were applied to the tissue sections for 1.5 hours at room temperature in the dark, and then the nuclei were counterstained with DAPI. The slides were mounted with ProLong Gold Antifade Mountant (ThermoFisher Scientific). Whole tissue slices were scanned using a NanoZoomer 2.0HT (Hamamatsu), and 3-D acquisitions were achieved with a confocal microscope SP5 (Leica). Mouse tissue stains (hematoxylin and eosin H&E, PAS, Alcian Blue) were performed using the LEICA ST5020-CV5030 automated stainer (Leica Biosystems, Wetzlar, Germany).

Image extraction and cell count

Image acquisition was obtained with a NanoZoomer from Hamamatsu. For each acquired image, the user must visualize the ndpi files using "NDP.view2" software (Hamamatsu). Interesting parts of the virtual slides were manually selected using regions of interests (ROIs). The following steps were developed using QuantaCell custom-made software solutions (MATLAB scripts and C++/OpenCV programs). Virtual images were automatically cropped inside the user-defined region and exported into jpg files at a 20x resolution. A semiautomatic sample detection was performed as follows: a gray image (named im_gray) was calculated from the original images (named im_orig), im_gray was filtered with morphological mathematics to make it homogeneous, and the automatic threshold value (named th) was calculated on im_gray using the Otsu method. Manual correction of th was possible with user intervention. A binary mask (named mask_sample) was calculated using th on im_gray. In mask_sample, small objects <7500 µm² were removed, and semiautomatic epidermal detection was performed. Green images (named im_green) were extracted from im_orig, and im_green was filtered with morphological mathematics to make it homogeneous. The automatic threshold value (named th_green) was calculated on im_green using the Otsu method, and manual correction of th_green was possible with user intervention. A binary

mask (named mask_epiderma) was calculated using th_green on im_green (mask_epiderma was restricted inside mask_sample). If several objects were present in mask_epiderma, then the object closest to the sample border was kept (to separate the epiderma from the internal green islet). A manual procedure was sometimes necessary to manually redraw mask_epiderma. It was useful for very inhomogeneous epidermis.

Automatic cell quantification was performed on the processed images. Then, blue images (named im_blue) were extracted from im_orig, and automatic nuclei detection was performed to individualize each nuclei from im_blue. This process was achieved using image smoothing (to remove noise), binarization, a watershed strategy to separate contiguous nuclei, and rejection of nuclei that were too small. The obtained image of the nuclei was named nuclei_mask. A donut shape with a width of 3.5 µm was generated around the nuclei to define the cytoplasmic area. The cell mask (named cell_mask) was the union of nuclei_mask and the donut-shaped mask. Intensity statistics using the averages among the pixel intensities were calculated for each cell in the whole cell (nuclei + cytoplasm) and for each fluorescent channel; for each cell, the closest distance to the epidermis was calculated, and the position in the tissue was recorded (in the epidermis, “epidermis islet” or dermis). Cell classification was performed according to 3 parameters: (i) whether the cell was in the epidermis or dermis; (ii) whether the cell was positive in red or negative in red and/or green (red positivity threshold was calculated as the median value for all cells of the sample + 10 fluorescent intensity units, and green positivity threshold was calculated as the median value for all cells of the sample + 50 fluorescent intensity units); and (iii) whether the cell was positive in green or negative in green. The following class counts were measured: cell count in epidermis, green positive cell count in epidermis, red negative cell count in epidermis, green positive and red negative count in epidermis, cell count in dermis, green positive cell count in dermis, red negative cell count in dermis, and green positive and red negative count in dermis. Statistics were exported in

Excel files for further exploitation, and montage images were automatically generated to represent the sample boundaries, epidermis and cell classes.

Cells were considered positive ILC2 when they had a nucleus surrounded by green fluorescence without any red.

Quantitative-Reverse Transcription-PCR (Q-RT-PCR)

RNA was purified from ILC subsets and fibroblasts using an RNeasy Plus Micro Kit (Qiagen), and the RNA concentration and purity were assessed using a Spectrophotometer DS11 (Denovix). The RNA integrity number (RIN) was assessed using an Agilent 2200 TapeStation (Agilent Technologies). All procedures were performed according to the manufacturer's instructions.

Total RNA was converted to cDNA using GoScript Reverse Transcription (Promega™). qPCR was performed using GoTaq Master Mix (all reagents were purchased from Promega™). The following targets were analyzed: *Tbet*, *GATA3*, *RORγt*, *COL1A1*, *COL1A2*, *FN1*, *IL10*, *LTC4S* and MMP1. The mRNA levels were normalized to *18S* rRNA and *RPLP0*.

Samples were distributed in duplicate in a 384-well plate using an Epmotion 5073 automated pipetting system (Eppendorf). Real-time quantitative PCR was performed using a CFX384 thermocycler (Bio-Rad™).

The data were analyzed using Bio-Rad™ CFX Manager software (Bio-Rad™), and differential expression was evaluated according to the ΔΔCt method.

For the reverse transcription quantitative PCR (RTqPCR) analysis of transcription factors, samples from 6 different donors were mixed at the same time. After sorting, the different subtypes of ILCs were separated into two fractions: one part was for the study of transcription factors at day 0 (D0) while the second part was expanded for 20 days for the study of transcription factors at day 20 (D20). The primers used in this study are listed in Table E1.

Collagen ELISA

The collagen production by dermal fibroblasts from HDs were assessed with the DuoSet® ELISA "Human Pro-Collagen I α1" (R&D Systems). Culture conditions were prepared as described by Dufour *et al.*[7]. Fibroblasts were used at passage 5–8 and cultured in DMEM containing 10% FCS, 1% non-essential amino acids, 1% l-glutamine, 1% sodium pyruvate, 50 U/ml penicillin, and 50 µg/ml streptomycin. Twenty thousand cells/well were seeded in 96-well plates for 24 hours, then starved for 16 hours in the absence of FCS, followed by stimulation with 50% of ILC2 supernatants in DMEM containing 1% FCS, 25 µg/ml L-ascorbic acid, 3.4 µg/ml α-ketoglutaric acid, and 50 µg/ml β-amino propionitrile to favor collagen maturation, as well as 50 U/ml penicillin and 50 µg/ml streptomycin. When used, cytokines or antibodies were added for 30 minutes to ILC2 supernatants before stimulation. Culture supernatants were harvested after 48 hours.

Average growth rate

The proliferation of fibroblasts was followed by live-cell imaging (Incucyte® ZOOM, Essen BioScience) for 48h. The average growth rate was calculated from the slope of the growth curves. For this assay, 2000 cells/well were seeded in 96-well plates for 24 hours, then starved for 16 hours in the absence of FCS, followed by stimulation with 50% of ILC2 supernatants in DMEM containing 0% FCS and 50 U/ml penicillin and 50 µg/ml streptomycin. When used, cytokines or antibodies were added for 30 minutes to ILC2 supernatants before stimulation.

Myofibroblasts differentiation

The differentiation of fibroblast into myofibroblasts was evaluated 72h post stimulation by flow cytometry analysis from fixed and permeabilized-cells stained with human alpha-

Smooth Muscle Actin APC-conjugated antibody (R&D Systems). For this assay, 20 000 cells/well were seeded in 24-well plates until the confluence was reached. Then, cells were starved for 24 hours in the absence of FCS, followed by stimulation with 50% of ILC2 supernatants in DMEM containing 0% FCS and 50 U/ml penicillin and 50 µg/ml streptomycin. When used, cytokines or antibodies were added for 30 minutes to ILC2 supernatants before stimulation.

RNA sequencing (RNAseq)

5.10^4 ILC2 were incubated at 37°C for 48 hours with or without recombinant TGFβ (R&D systems) at 10 ng/mL. After incubation, cells were washed with PBS and lysed using QIAGEN RNeasy micro kit plus®. RNA were subsequently extracted using the manufacturer's instructions. After RNA extraction, RNA concentrations were obtained using nanodrop or a fluorometric Qubit RNA assay (Life Technologies, Grand Island, New York, USA). The quality of the RNA (RNA integrity number) was determined on the Agilent 2100 Bioanalyzer (Agilent Technologies, Palo Alto, CA, USA) as per the manufacturer's instructions.

To construct the libraries, 800 ng of high quality total RNA sample (RIN >8) was processed using TruSeq Stranded mRNA kit (Illumina) according to manufacturer instructions. Briefly, after purification of poly-A containing mRNA molecules, mRNA molecules are fragmented and reverse- transcribed using random primers. Replacement of dTTP by dUTP during the second strand synthesis will permit to achieve the strand specificity. Addition of a single A base to the cDNA is followed by ligation of Illumina adapters.

Libraries were quantified by qPCR using the KAPA Library Quantification Kit for Illumina Libraries (KapaBiosystems, Wilmington, MA) and library profiles were assessed using the DNA High Sensitivity LabChip kit on an Agilent Bioanalyzer. Libraries were sequenced on

an Illumina Nextseq 500 instrument using 75 base-lengths read V2 chemistry in a paired-end mode.

RNASeq analysis

Illumina paired-end reads were quality filtered with fastp 0.20.0[8]. Mapping against the human GRCh38.primary assembly genome was performed with STAR 2.7.1a[9] by using the ENCODE options. "--quantMode GeneCounts" option was used to make STAR count the number of reads per gene while mapping. Differential expression study was performed by using R package DESeq2 (v1.14.1 with R version 3.3.2)[10]. Pre-filtering was carried out on the total counting matrix in order to keep only the genes having at least 10 reads detected (here : 18,726 genes). Differentially expressed genes between non activated cells and activated with TGFβ were filtered at a threshold of the adjusted pvalue (padj) < 0.01 (here : 3,134 genes). These differentially expressed genes were plotted as a heatmap with the R pheatmap library (version 1.0.12). {https://CRAN.R-project.org/package=pheatmap}. Subsequently, these genes were subjected to an enrichment analysis using the R Gprofiler2 library (version 0.1.8) {https://CRAN.R-project.org/package=gprofiler2} on the latest available versions of the following databases : Gene Ontology Molecular Function, Biological Process, Cellular Component ; Biological Pathways : KEGG ; Reactome ; WikiPathways ; Regulatory motifs in DNA : TRANSFAC , miRTarBase ; Protein databases : Human Protein Atlas, CORUM ; Human phenotype ontology. The results were filtered at a threshold of the adjusted pvalue (padj) < 0.05.

Statistical analysis

Statistical analyses were performed using GraphPad Prism (La Jolla, CA). For distributions that satisfied the Kolmogorov–Smirnov normality test, a two-tailed Student t-test for unpaired

or paired samples and one-way repeated-measures ANOVA followed by Bonferroni correction were used to compare the different populations according to the experimental design. When the normality test was not satisfied, the Mann-Whitney, Wilcoxon and Kruskal-Wallis tests were used. Correlations were analyzed using the Spearman test. A P-value < 0.05 indicated statistical significance.

REFERENCES

1 van den Hoogen F, Khanna D, Fransen J, *et al.* 2013 classification criteria for systemic sclerosis: an American College of Rheumatology/European League against Rheumatism collaborative initiative. *Arthritis Rheum* 2013;**65**:2737–47. doi:10.1002/art.38098

2 Kavian N, Marut W, Servettaz A, *et al.* Reactive oxygen species-mediated killing of activated fibroblasts by arsenic trioxide ameliorates fibrosis in a murine model of systemic sclerosis. *Arthritis Rheum* 2012;**64**:3430–40. doi:10.1002/art.34534

3 Vallentin B, Barlogis V, Piperoglou C, *et al.* Innate Lymphoid Cells in Cancer. *Cancer Immunol Res* 2015;**3**:1109–14. doi:10.1158/2326-6066.CIR-15-0222

4 Ohne Y, Silver JS, Thompson-Snipes L, *et al.* IL-1 is a critical regulator of group 2 innate lymphoid cell function and plasticity. *Nat Immunol* 2016;**17**:646–55. doi:10.1038/ni.3447

5 Truchetet M-E, Brembilla N-C, Montanari E, *et al.* Interleukin-17A+ cell counts are increased in systemic sclerosis skin and their number is inversely correlated with the extent of skin involvement. *Arthritis Rheum* 2013;**65**:1347–56. doi:10.1002/art.37860

6 Truchetet M-E, Demoures B, Eduardo Guimaraes J, *et al.* Platelets Induce Thymic Stromal Lymphopoietin Production by Endothelial Cells: Contribution to Fibrosis in Human Systemic Sclerosis. *Arthritis Rheumatol Hoboken NJ* 2016;**68**:2784–94. doi:10.1002/art.39817

7 Dufour AM, Borowczyk-Michalowska J, Alvarez M, *et al.* IL-17A Dissociates Inflammation from Fibrogenesis in Systemic Sclerosis. *J Invest Dermatol* 2020;**140**:103-112.e8. doi:10.1016/j.jid.2019.05.026

8 Chen S, Zhou Y, Chen Y, *et al.* fastp: an ultra-fast all-in-one FASTQ preprocessor. *Bioinforma Oxf Engl* 2018;**34**:i884–90. doi:10.1093/bioinformatics/bty560

9 Dobin A, Davis CA, Schlesinger F, *et al.* STAR: ultrafast universal RNA-seq aligner. *Bioinforma Oxf Engl* 2013;**29**:15–21. doi:10.1093/bioinformatics/bts635

10 Love MI, Huber W, Anders S. Moderated estimation of fold change and dispersion for RNA-seq data with DESeq2. *Genome Biol* 2014;**15**:550. doi:10.1186/s13059-014-0550-8

FIGURES

Online supplemental figure 1. Absolute values of ILCs in the blood of patients with systemic sclerosis (SSc) and healthy donors (HDs).

(A) FMOs and gating strategy: the FMO for the lineage negative cells (FMO Lin) was gated on $CD45^+$ cells from the peripheral blood. The scale allows the visualization of the dimensions of the gates and the proper set of the gate for ILCs. The FMO for CRTH2 (FMO CRTH2) and CD117 (FMO CD117) are gated on ILCs. Then, ILCs subsets are shown according to the FMO of CRTH2 and CD117. (B) The whole set of cells identified by our gating strategy as ILCs show a similar distribution, making it a homogeneous population. (C) Absolute values of ILCs in HD and SSc blood. (D) Absolute values of ILC subsets in HD and SSc blood. (E) Percentage of $KLRG1^+$ ILC2 in HD and SSc blood. (F) Absolute number of circulating ILC2 in patients with limited (Rodnan <10) and diffuse (Rodnan >10) SSc. Bar graphs show data as the mean ± SEM (n=59 and 73 for HDs and SSc patients respectively). Comparison between groups was calculated using Mann-Whitney test. ***, $P < 0.001$.

Online supplemental figure 2. Characterization of ILCs in the skin of patients with systemic sclerosis (SSc) and healthy donors (HDs).

(A) FMOs and gating strategy. (B) Percentage of ILC1 in HD and SSc skin. (C) Correlation between percentage of cutaneous ILC1 and the extent of fibrosis (mRSS). (D) Percentage of ILC2 per total cell count in the dermis of HD and SSc skin. Bar graphs show data as the mean ± SEM (n=17 for HD and SSc in flow cytometry and n=17 and 30 for HD and SSc, respectively for immunofluorescence). Comparison between groups was calculated using Mann-Whitney test. ***, $P < 0.001$.

Online supplemental figure 3. Characterization of ILC2 after sorting and 20 days of amplification.

(A) Representative dot blot of ILC2 ($CD45^+Lin^-CD127^+CRTH2^+$) sorting. (B) Verification of ILC2 phenotype after 20 days of amplification with IL2 and IL1β. (C) RTqPCR analysis of ILC2 for *Tbet*, *GATA3* and *RORγt* after amplification. Relative expressions of *Tbet*, *GATA3* and *RORγt* were represented using 1/ΔCt. Bar graphs show data as the mean ± SEM (n=3).

Online supplemental figure 4. Heat map of gene expression between TGFβ-stimulated ILC2 and unstimulated ILC2.

(A) Heat map of 2840 genes differentially expressed (p adjusted value < 0.01) between TGFβ-stimulated ILC2 (n=3) and unstimulated ILC2 (n=3). (B) Q-RT-PCR analysis of *IL10* and *LTC4S* mRNA expression (n=4). Comparison between groups was calculated using Mann-Whitney test. *, $P < 0.05$.

Online supplemental figure 5. Characterization of ILCs in skin of HOCL-treated mice and control mice.

(A) Absolute count of ILC2 and (B) ILCs in skin of control and HOCl mice at day 42. (C) Percentage of ILC2 among $CD45^+$ lymphoid cells in control and HOCl skin mice at day 21. (D) Absolute count of ILC2 in skin of control and HOCl mice at day 21. (E) Skin thickness and (F) collagen assay in skin of control and HOCl mice. Bar graphs show data as the mean ± SEM (n=10 for control mice and n=9 to 10 for HOCl mice respectively in D21 and D42). Comparison between groups was calculated using Mann-Whitney test. **, $P < 0.01$; ***, $P < 0.001$; ****, $P < 0.0001$.

TABLES

Table E1. Primers used in the study.

mRNA	***PRIMER***	***TM (SA)***	**Amplicon**
MMP1	**F:** GGAGGAAAAGCAGCTCAAGAAC	62,1°C	50pb
	R: TCCAGGGTGACACCAGTGACT	63,2°C	
COL1A1	**F:** CCCTCCTGACGCACGG	58,4°C	66pb
	R: GTGATTGGTGGGATGTCTTCGT	62,1°C	
COL1A2	**F:** CTGTAAGAAAGGGCCCAGCC	62,5°C	50pb
	R: GACCCCTTTCTCCACGTGG	61,6°C	
FN1	**F:** GGGAGAATAAGCTGTACCATCG	59°C	129pb
	R: TCCATTACCAAGACACACACACT	59°C	
IL10	**F:** TGCCTTCAGCAGAGTGAAGA	59°C	103pb
	R: GCAACCCAGGTAACCCTTAAA	60°C	
LTC4S	**F:** ACCATGAAGGACGAGGTAGC	59°C	77pb
	R: TGCAGGGAGAAGTAGGCTTG	60°C	
RORγt	**F:** CTGGGCATGTCCCGAGATG	62.2°C	133pb
	R: GAGGGGTCTTGACCACTGG	61.3°C	
GATA3	**F:** GCCCCTCATTAAGCCCAAG	65,6°C	80pb
	R: TTGTGGTGGTCTGACAGTTCG	66,3°C	
Tbet	**F:** GTCCAACAATGTGACCCAGAT	60°C	75pb
	R: ACCTCAACGATATGCAGCCG	62.4°C	
HOUSEKEEPING G.	***PRIMER***	***TM (SA)***	**Amplicon**
18s	**F:** TGCCATCACTGCCATTAAG	65.9°C	61pb
	R: TGCTTTCCTCAACACCACATG	66°C	
RPLP0	**F:** GCAGCATCTACAACCCTGAAG	60.7°C	87pb
	R: CACTGGCAACATTGCGGAC	62°C	

399 **Table E2. Reagents and products used in this study.**

REAGENT or RESSOURCE	SOURCE	IDENTIFIER
Antibodies		
anti-human CD3 APC	Miltenyi	BW264/56
anti-human CD5 APC	Miltenyi	UCHT2
anti-human CD14 APC	Miltenyi	TUK4
anti-human CD16APC	Miltenyi	REA423
anti-human CD19APC	Miltenyi	LT19
anti-human CD31APC	Miltenyi	AC128
anti-human CD34APC	Miltenyi	AC136
anti-human CD45APC	Miltenyi	5B11
anti-human CD56APC	Miltenyi	AF12-7H3
anti-human CD94APC	Miltenyi	REA113
anti-human CD123 APC	Miltenyi	AC145
anti-human CD303APC	Miltenyi	AC144
anti-humanTCRabAPC	Miltenyi	BW242/412
anti-humanTCRgdAPC	Miltenyi	11F2
anti-human CD117Pe-Vio770	Miltenyi	A3C6E2
anti-humanCD127Pe-Vio665	Miltenyi	MB15-18C9
anti-humanCLAFITC	Miltenyi	HECA-452
anti-humanCCR10PerCP/Cy5.5	BD	1B5
anti-humanCCR6 BV786	BD	11A9
anti-humanHLA-DRPerCP/Cy5.5	BD	L243
anti-humanOX40L PE	Abcam	ANC10G1
anti-humanTSLPR PE	BD	1F11
anti-humanCRTH2BV421	BD	BM16
Anti-human FcεR1 APC	eBioscience	AER-37
anti-humanKLRG1FITC	eBioscience	13F12F2
anti-humanaSMAAPC	R&D Systems	1A4
anti-human CD1aAPC	Beckman Coulter	BL6
anti-human CD3 APC	Beckman Coulter	UCHT1
anti-human CD11c APC	Beckman Coulter	BU15
anti-human CD14APC	Beckman Coulter	RMO52
anti-human CD16APC	Beckman Coulter	3G8
anti-human CD19APC	Beckman Coulter	J3-119
anti-human CD34APC	Beckman Coulter	581
anti-human CD94APC	Beckman Coulter	HP-3B1
anti-human CD123APC	Beckman Coulter	AC145
anti-human CD45KO	Beckman Coulter	J33
anti-human CD117PE/Cyy5.5	Beckman Coulter	104D2D1
anti-human CD127APC/AF700	Beckman Coulter	R34.34
anti-humanCRTH2 FITC	Beckman Coulter	BM16
anti-human CD5 APC	BD	UCHT2
anti-human FcεR1 APC	eBioscience	AER-37
anti-humanCD31APC	Miltenyi	AC128
Anti-mouse ST2	Biolegend	DIH9
anti-mouse CD117	Miltenyi	REA791

Anti-mouse CD25 PE	Miltenyi	REA568
Anti-mouse CD45	Miltenyi	REA737
Anti-mouse KLRG1	Miltenyi	REA1016
Anti-mouse CD127	Miltenyi	REA680
anti-mouse CD5 Biotin	Miltenyi	REA421
Anti-mouse CD3e Biotin	Miltenyi	17A2
anti-mouse LY6G/C Biotin	Miltenyi	REA526
anti-mouse CD45R Biotin	Miltenyi	REA755
anti-mouse CD11b Biotin	Miltenyi	REA592
anti-mouse Ter-119 Biotin	Miltenyi	TER119
Rabbit anti-human CRTH2	Novus Biologicals	GPR44
Human anti-human CD3	Abcam	PS1
Human anti-human CD11b	Novus Biologicals	CL1719
Human anti-human FcεR1	Thermo Fisher	9E1
Chemicals, Peptides, and Recombinant Proteins		
Human recombinant IL33	Miltenyi	
Human recombinant TGFb	R&D System	
Human recombinant IL4	Miltenyi	
Human recombinant TSLP	R&D System	
Human recombinant IL25	Miltenyi	
Human recombinant IL2	Miltenyi	
Human recombinant IL1b	R&D System	
Human recombinant IL10	Miltenyi	
Mouse recombinant IL10	Miltenyi	
Pirfenidone	Hospital of Bordeaux	
KH_2PO_4	Sigma-Aldrich	
NaClO	Sigma-Aldrich	

400

401 **Table E3. Gene Ontology analysis. List of the first 50-upregulated biological processes.**

source	term_name	term_id	padj
GO:BP	positive regulation of GTPase activity	GO:0043547	2.64E-06
GO:BP	regulation of GTPase activity	GO:0043087	2.64E-06
GO:BP	regulation of signaling	GO:0023051	3.49E-06
GO:BP	regulation of response to stimulus	GO:0048583	7.43E-06
GO:BP	regulation of cell communication	GO:0010646	8.02E-06
GO:BP	regulation of signal transduction	GO:0009966	1.06E-05
GO:BP	myeloid cell differentiation	GO:0030099	1.06E-05
GO:BP	leukocyte differentiation	GO:0002521	1.35E-05
GO:BP	regulation of hemopoiesis	GO:1903706	1.35E-05
GO:BP	immune system development	GO:0002520	2.29E-05
GO:BP	hemopoiesis	GO:0030097	4.30E-05
GO:BP	regulation of leukocyte differentiation	GO:1902105	7.23E-05
GO:BP	negative regulation of response to stimulus	GO:0048585	7.23E-05
GO:BP	hematopoietic or lymphoid organ development	GO:0048534	1.42E-04
GO:BP	T cell activation	GO:0042110	1.42E-04
GO:BP	lymphocyte activation	GO:0046649	1.98E-04
GO:BP	regulation of cell-cell adhesion	GO:0022407	2.23E-04
GO:BP	immune system process	GO:0002376	2.26E-04
GO:BP	T cell differentiation	GO:0030217	2.26E-04
GO:BP	positive regulation of hydrolase activity	GO:0051345	2.55E-04
GO:BP	regulation of lymphocyte differentiation	GO:0045619	2.63E-04
GO:BP	regulation of B cell proliferation	GO:0030888	3.43E-04
GO:BP	intracellular signal transduction	GO:0035556	3.43E-04
GO:BP	leukocyte activation	GO:0045321	4.06E-04
GO:BP	cell activation	GO:0001775	4.13E-04
GO:BP	positive regulation of cell-cell adhesion	GO:0022409	4.13E-04
GO:BP	regulation of cell activation	GO:0050865	4.13E-04
GO:BP	positive regulation of cell adhesion	GO:0045785	4.31E-04
GO:BP	regulation of T cell activation	GO:0050863	4.86E-04
GO:BP	myeloid leukocyte differentiation	GO:0002573	5.85E-04
GO:BP	positive regulation of leukocyte differentiation	GO:1902107	6.45E-04
GO:BP	osteoclast differentiation	GO:0030316	6.45E-04
GO:BP	positive regulation of hemopoiesis	GO:1903708	6.45E-04
GO:BP	regulation of cell adhesion	GO:0030155	6.45E-04
GO:BP	regulation of alpha-beta T cell activation	GO:0046634	6.69E-04
GO:BP	regulation of leukocyte activation	GO:0002694	6.91E-04
GO:BP	granzyme-mediated programmed cell death signaling pathway	GO:0140507	7.23E-04
GO:BP	negative regulation of transferase activity	GO:0051348	7.37E-04
GO:BP	regulation of lymphocyte activation	GO:0051249	7.81E-04
GO:BP	regulation of T cell differentiation	GO:0045580	8.71E-04
GO:BP	negative regulation of signaling	GO:0023057	9.46E-04
GO:BP	regulation of osteoclast differentiation	GO:0045670	1.11E-03
GO:BP	negative regulation of immune response	GO:0050777	1.11E-03
GO:BP	regulation of leukocyte cell-cell adhesion	GO:1903037	1.11E-03
GO:BP	cell adhesion	GO:0007155	1.17E-03
GO:BP	negative regulation of signal transduction	GO:0009968	1.18E-03
GO:BP	leukocyte cell-cell adhesion	GO:0007159	1.21E-03
GO:BP	regulation of tumor necrosis factor superfamily cytokine production	GO:1903555	1.21E-03
GO:BP	regulation of intracellular signal transduction	GO:1902531	1.21E-03
GO:BP	negative regulation of tumor necrosis factor production	GO:0032720	1.21E-03

402

403 **Table E4. Gene Ontology analysis. List of upregulated cellular components.**

source	term_name	term_id	padj
GO:CC	plasma membrane	GO:0005886	3.41E-05
GO:CC	cell periphery	GO:0071944	3.41E-05
GO:CC	side of membrane	GO:0098552	2.02E-04
GO:CC	external side of plasma membrane	GO:0009897	4.01E-04
GO:CC	specific granule membrane	GO:0035579	5.54E-04
GO:CC	membrane microdomain	GO:0098857	9.49E-04
GO:CC	membrane raft	GO:0045121	9.49E-04
GO:CC	microvillus	GO:0005902	1.04E-03
GO:CC	cytoplasmic vesicle	GO:0031410	1.19E-03
GO:CC	intracellular vesicle	GO:0097708	1.19E-03
GO:CC	intrinsic component of plasma membrane	GO:0031226	1.22E-03
GO:CC	focal adhesion	GO:0005925	1.22E-03
GO:CC	protein complex involved in cell adhesion	GO:0098636	1.22E-03
GO:CC	cell-substrate junction	GO:0030055	1.90E-03
GO:CC	cell surface	GO:0009986	2.13E-03
GO:CC	integral component of plasma membrane	GO:0005887	3.57E-03
GO:CC	Golgi apparatus	GO:0005794	4.45E-03
GO:CC	condensed chromosome kinetochore	GO:0000777	4.72E-03
GO:CC	bounding membrane of organelle	GO:0098588	5.46E-03
GO:CC	integrin complex	GO:0008305	5.46E-03
GO:CC	ruffle membrane	GO:0032587	5.97E-03
GO:CC	endosome	GO:0005768	6.94E-03
GO:CC	ruffle	GO:0001726	6.94E-03
GO:CC	condensed chromosome, centromeric region	GO:0000779	8.41E-03
GO:CC	condensed nuclear chromosome kinetochore	GO:0000778	8.41E-03
GO:CC	plasma membrane raft	GO:0044853	8.90E-03
GO:CC	specific granule	GO:0042581	9.61E-03
GO:CC	cytoplasmic vesicle membrane	GO:0030659	9.61E-03
GO:CC	protein serine/threonine phosphatase complex	GO:0008287	9.67E-03
GO:CC	phosphatase complex	GO:1903293	9.67E-03
GO:CC	histone locus body	GO:0035363	1.00E-02
GO:CC	condensed nuclear chromosome outer kinetochore	GO:0000942	1.07E-02
GO:CC	vesicle membrane	GO:0012506	1.07E-02
GO:CC	integrin alphaM-beta2 complex	GO:0034688	1.23E-02
GO:CC	cytoplasm	GO:0005737	1.23E-02
GO:CC	growth cone	GO:0030426	1.35E-02
GO:CC	tertiary granule	GO:0070820	1.42E-02
GO:CC	adherens junction	GO:0005912	1.42E-02
GO:CC	nuclear body	GO:0016604	1.42E-02
GO:CC	recycling endosome	GO:0055037	1.61E-02
GO:CC	cell leading edge	GO:0031252	1.89E-02
GO:CC	midbody	GO:0030496	1.91E-02
GO:CC	protein phosphatase type 2A complex	GO:0000159	1.92E-02
GO:CC	site of polarized growth	GO:0030427	1.93E-02
GO:CC	kinetochore	GO:0000776	2.01E-02
GO:CC	nucleoplasm	GO:0005654	2.01E-02
GO:CC	fibrillar center	GO:0001650	2.41E-02
GO:CC	cytosol	GO:0005829	2.41E-02
GO:CC	endomembrane system	GO:0012505	2.44E-02
GO:CC	actin-based cell projection	GO:0098858	2.64E-02
GO:CC	cleavage furrow	GO:0032154	2.67E-02
GO:CC	anchoring junction	GO:0070161	2.67E-02
GO:CC	perinuclear region of cytoplasm	GO:0048471	3.01E-02
GO:CC	transcription factor AP-1 complex	GO:0035976	3.47E-02
GO:CC	cell projection membrane	GO:0031253	3.49E-02

GO:CC	vesicle	GO:0031982	3.71E-02
GO:CC	phagolysosome	GO:0032010	3.71E-02
GO:CC	myosin complex	GO:0016459	3.71E-02
GO:CC	F-actin capping protein complex	GO:0008290	3.76E-02
GO:CC	immunological synapse	GO:0001772	4.01E-02
GO:CC	early endosome	GO:0005769	4.01E-02
GO:CC	tertiary granule membrane	GO:0070821	4.01E-02
GO:CC	**heteromeric SMAD protein complex**	**GO:0071144**	**4.01E-02**
GO:CC	axonal growth cone	GO:0044295	4.16E-02
GO:CC	beta-catenin destruction complex	GO:0030877	4.16E-02
GO:CC	protein kinase 5 complex	GO:0016533	4.21E-02
GO:CC	endosome membrane	GO:0010008	4.22E-02
GO:CC	condensed chromosome	GO:0000793	4.22E-02
GO:CC	cytoplasmic side of dendritic spine plasma membrane	GO:1990780	4.22E-02
GO:CC	transcription elongation factor complex	GO:0008023	4.27E-02
GO:CC	**SMAD protein complex**	**GO:0071141**	**4.45E-02**
GO:CC	muscle cell projection	GO:0036194	4.61E-02
GO:CC	muscle cell projection membrane	GO:0036195	4.61E-02
GO:CC	centrosome	GO:0005813	4.61E-02

404

405 **Table E5. Gene Ontology analysis. List of the first 50-upregulated molecular function.**

source	term_name	term_id	padj
GO:MF	GTPase regulator activity	GO:0030695	1.17E-07
GO:MF	GTPase activator activity	GO:0005096	1.18E-06
GO:MF	nucleoside-triphosphatase regulator activity	GO:0060589	1.18E-06
GO:MF	enzyme binding	GO:0019899	4.02E-04
GO:MF	enzyme regulator activity	GO:0030234	6.60E-04
GO:MF	enzyme activator activity	GO:0008047	8.88E-04
GO:MF	kinase activity	GO:0016301	4.11E-03
GO:MF	C-C chemokine binding	GO:0019957	5.60E-03
GO:MF	kinase regulator activity	GO:0019207	5.64E-03
GO:MF	cell adhesion molecule binding	GO:0050839	9.72E-03
GO:MF	GTPase activity	GO:0003924	9.72E-03
GO:MF	**SMAD binding**	**GO:0046332**	**9.72E-03**
GO:MF	protein kinase regulator activity	GO:0019887	9.72E-03
GO:MF	phosphatidylinositol 3-kinase binding	GO:0043548	9.72E-03
GO:MF	kinase binding	GO:0019900	9.72E-03
GO:MF	**I-SMAD binding**	**GO:0070411**	**9.72E-03**
GO:MF	chemokine binding	GO:0019956	9.72E-03
GO:MF	protein kinase binding	GO:0019901	9.72E-03
GO:MF	kinase inhibitor activity	GO:0019210	9.72E-03
GO:MF	death receptor activity	GO:0005035	1.08E-02
GO:MF	actin filament binding	GO:0051015	1.08E-02
GO:MF	phosphotransferase activity, alcohol group as acceptor	GO:0016773	1.08E-02
GO:MF	protein kinase inhibitor activity	GO:0004860	1.10E-02
GO:MF	protein tyrosine/threonine phosphatase activity	GO:0008330	1.11E-02
GO:MF	immune receptor activity	GO:0140375	1.28E-02
GO:MF	cytokine receptor activity	GO:0004896	1.30E-02
GO:MF	C-C chemokine receptor activity	GO:0016493	1.58E-02
GO:MF	coreceptor activity	GO:0015026	1.58E-02
GO:MF	G protein-coupled chemoattractant receptor activity	GO:0001637	1.58E-02
GO:MF	chemokine receptor activity	GO:0004950	1.58E-02
GO:MF	cadherin binding	GO:0045296	1.88E-02
GO:MF	tumor necrosis factor-activated receptor activity	GO:0005031	1.88E-02
GO:MF	phosphoric ester hydrolase activity	GO:0042578	2.03E-02
GO:MF	15-hydroxyprostaglandin dehydrogenase (NAD+) activity	GO:0016404	2.03E-02
GO:MF	UDP-N-acetylglucosamine-lysosomal-enzyme N-acetylglucosaminephosphotransferase activity	GO:0003976	2.03E-02
GO:MF	C-X-C chemokine receptor activity	GO:0016494	2.03E-02
GO:MF	inorganic phosphate transmembrane transporter activity	GO:0005315	2.09E-02
GO:MF	spectrin binding	GO:0030507	2.09E-02
GO:MF	phosphatidylinositol-4,5-bisphosphate phosphatase activity	GO:0106019	2.09E-02
GO:MF	transferase activity, transferring phosphorus-containing groups	GO:0016772	2.09E-02
GO:MF	protein domain specific binding	GO:0019904	2.18E-02
GO:MF	cytokine binding	GO:0019955	2.62E-02
GO:MF	MAP kinase phosphatase activity	GO:0033549	2.79E-02
GO:MF	actin binding	GO:0003779	2.79E-02
GO:MF	GTP binding	GO:0005525	3.79E-02
GO:MF	C-X-C chemokine binding	GO:0019958	3.79E-02
GO:MF	glycerophosphodiester phosphodiesterase activity	GO:0008889	3.79E-02
GO:MF	guanyl nucleotide binding	GO:0019001	3.79E-02
GO:MF	guanyl ribonucleotide binding	GO:0032561	3.79E-02
GO:MF	polyamine oxidase activity	GO:0046592	3.79E-02
GO:MF	virus receptor activity	GO:0001618	3.85E-02
GO:MF	purine ribonucleoside binding	GO:0032550	4.10E-02
GO:MF	exogenous protein binding	GO:0140272	4.10E-02
GO:MF	ubiquitin-like protein ligase binding	GO:0044389	4.27E-02

GO:MF	ribonucleoside binding	GO:0032549	4.27E-02
GO:MF	purine nucleoside binding	GO:0001883	4.27E-02
GO:MF	ubiquitin protein ligase binding	GO:0031625	4.27E-02
GO:MF	phosphatidylinositol phosphate 4-phosphatase activity	GO:0034596	4.30E-02
GO:MF	MAP kinase tyrosine/serine/threonine phosphatase activity	GO:0017017	4.30E-02
GO:MF	phosphatidylinositol-3,4,5-trisphosphate binding	GO:0005547	4.35E-02
GO:MF	cytoskeletal protein binding	GO:0008092	4.48E-02
GO:MF	growth factor activity	GO:0008083	4.71E-02
GO:MF	nucleoside binding	GO:0001882	4.71E-02
GO:MF	AP-1 adaptor complex binding	GO:0035650	4.71E-02

406

407 **Table E6. miRTarBase analysis.**

source	term_name	term_id	padj
MIRNA	hsa-miR-519d-3p	MIRNA:hsa-miR-519d-3p	4.17E-02

408

409 **Table E7. Transfac analysis. List of the first 50-upregulated transcription factors.**

source	term_name	term_id	padj
TF	Factor: E2F-3; motif: GGCGGGN; match class: 1	TF:M02089_1	2.17E-16
TF	Factor: Sp1; motif: NGGGGGCGGGGCCNGGGGGGGG; match class: 1	TF:M10071_1	3.79E-16
TF	Factor: ETF; motif: GVGGMGG; match class: 1	TF:M00695_1	1.81E-14
TF	Factor: BTEB1; motif: GGGGGCGGGGCNGSGGGNGS; match class: 1	TF:M09723_1	2.29E-14
TF	Factor: GKLF; motif: GCCMCRCCCNNN; match class: 1	TF:M01588_1	3.07E-14
TF	Factor: SP2; motif: GNNGGGGGCGGGGSN; match class: 1	TF:M03807_1	5.65E-14
TF	Factor: sp4; motif: NNGNARGRGGCGGRGCNNRR; match class: 1	TF:M10072_1	5.65E-14
TF	Factor: Sp2; motif: NYSGCCCCGCCCCCY	TF:M03567	7.44E-14
TF	Factor: KLF3; motif: NNNNNNGGGCGGGGCNNGN	TF:M09970	8.30E-14
TF	Factor: WT1; motif: CGCCCCCNCN; match class: 1	TF:M02036_1	9.64E-14
TF	Factor: WT1; motif: GNGGGGGCGGGG; match class: 1	TF:M03893_1	1.79E-13
TF	Factor: Sp1; motif: GGGGCGGGGC; match class: 1	TF:M00931_1	1.79E-13
TF	Factor: Sp1; motif: GGGGCGGGGT; match class: 1	TF:M00008_1	2.66E-13
TF	Factor: Sp1; motif: NNGGGGCGGGGNN; match class: 1	TF:M00932_1	2.82E-13
TF	Factor: SP1; motif: NCCCCKCCCCC; match class: 1	TF:M07226_1	3.11E-13
TF	Factor: KLF3; motif: NNNNNNGGGCGGGGCNNGN; match class: 1	TF:M09970_1	3.11E-13
TF	Factor: Sp1; motif: NGGGGCGGGGN; match class: 1	TF:M07395_1	5.26E-13
TF	Factor: BTEB2; motif: RGGGNGKGGN; match class: 1	TF:M07277_1	6.14E-13
TF	Factor: EKLF; motif: NGGGYGKGGCNNGG; match class: 1	TF:M09969_1	8.45E-13
TF	Factor: Sp1; motif: NGGGGGCGGGGCCNGGGGGGGG	TF:M10071	8.91E-13
TF	Factor: sp4; motif: NNNGCYCCGCCCCCY; match class: 1	TF:M10530_1	9.25E-13
TF	Factor: BTEB2; motif: RGGGNGKGGN	TF:M07277	9.68E-13
TF	Factor: Sp2; motif: GGSNNGGGGGCGGGGCCNGNGS	TF:M09658	1.13E-12
TF	Factor: AP-2rep; motif: NGGGGCGGGGC	TF:M09967	1.40E-12
TF	Factor: GKLF; motif: NNCCMCRCCCN; match class: 1	TF:M12173_1	1.43E-12
TF	Factor: Sp1; motif: NGGGGGCGGGGYN; match class: 1	TF:M00196_1	1.61E-12
TF	Factor: BTEB3; motif: CCNNSCCNSCCCCKCCCCC; match class: 1	TF:M09826_1	1.87E-12
TF	Factor: CPBP; motif: GNNRGGGHGGGGNNGGGRN; match class: 1	TF:M09973_1	1.87E-12
TF	Factor: AP-2; motif: GSCCSCRGGCNRNRNN; match class: 1	TF:M00800_1	1.87E-12
TF	Factor: TIEG1; motif: NCCCNSNCCCCGCCCCC; match class: 1	TF:M12351_1	2.05E-12
TF	Factor: AP-2; motif: MKCCCSCNGGCG; match class: 1	TF:M00189_1	2.21E-12
TF	Factor: SP2; motif: GNNGGGGGCGGGGSN	TF:M03807	3.75E-12
TF	Factor: BTEB1; motif: GGGGGCGGGGCNGSGGGNGS	TF:M09723	4.16E-12
TF	Factor: Sp1; motif: NGGGGGCGGGGYN	TF:M00196	4.64E-12
TF	Factor: BTEB2; motif: GCCCCRCCCH	TF:M07409	6.95E-12
TF	Factor: Sp2; motif: NYSGCCCCGCCCCCY; match class: 1	TF:M03567_1	7.16E-12
TF	Factor: Sp2; motif: GGGGCGGGG	TF:M10435	7.61E-12
TF	Factor: Sp1; motif: GGGGCGGGGC	TF:M07063	7.61E-12
TF	Factor: Sp1; motif: NGGGGCGGGGN	TF:M07395	8.20E-12
TF	Factor: Sp2; motif: GYCCCGCCYCYNNNN	TF:M07129	9.60E-12
TF	Factor: SP1; motif: NRGKGGGCGGGGCN; match class: 1	TF:M09765_1	1.11E-11
TF	Factor: BTEB2; motif: GCCCCRCCCH; match class: 1	TF:M07409_1	1.11E-11
TF	Factor: Sp1; motif: CCCCGCCCCN; match class: 1	TF:M00933_1	1.15E-11
TF	Factor: Egr-1; motif: GCGGGGGCGG; match class: 1	TF:M01873_1	1.18E-11
TF	Factor: SP1; motif: NRGKGGGCGGGGCN	TF:M09765	1.38E-11
TF	Factor: Sp1; motif: NNGGGGCGGGGNN	TF:M00932	1.77E-11
TF	Factor: Egr-1; motif: GCGGGGGCGG; match class: 1	TF:M07354_1	1.77E-11
TF	Factor: Sp3; motif: GGGGCGGGGSNN	TF:M07615	2.55E-11
TF	Factor: Egr-1; motif: GCGGGGGCGG	TF:M07354	2.91E-11
TF	Factor: AP-2rep; motif: NGGGGCGGGGC; match class: 1	TF:M09967_1	2.93E-11

410

411 **Table E8. List of the first 60 upregulated genes (red) and downregulated genes (green).**

Gene name	log2FoldChange	padj	Gene name	log2FoldChange	padj
QPCT	5.13	1.52E-121	*ST6GALNAC1*	-3.92	8.64E-53
CA10	4.18	2.46E-52	***IL10***	**-3.71**	**1.36E-51**
PRICKLE1	3.97	3.93E-63	*ARG2*	-3.23	2.06E-48
PMEPA1	3.95	1.61E-176	*SOCS3*	-3.16	1.44E-79
NKD1	3.91	2.58E-82	*NHSL2*	-2.91	5.21E-52
RGS16	3.83	1.64E-132	*GZMA*	-2.87	2.96E-48
CSPG5	3.83	8.25E-55	*AL121933.2*	-2.81	7.12E-67
AFAP1	3.35	5.71E-33	*SELL*	-2.67	1.32E-31
SH2D4A	3.10	4.02E-66	*AIRE*	-2.62	1.86E-17
SLC6A4	2.87	7.09E-19	*PAPSS2*	-2.52	1.03E-24
CDK5R1	2.86	3.48E-57	*SH3RF3*	-2.48	1.55E-29
ATP10D	2.77	4.07E-33	*AXIN2*	-2.47	5.65E-18
INAVA	2.76	2.24E-20	*ROPN1L*	-2.42	1.13E-34
GPR35	2.75	1.55E-22	*LINC01943*	-2.38	8.35E-24
TBC1D16	2.73	8.80E-179	*SULT1B1*	-2.37	5.27E-13
PNMA8C	2.71	6.68E-27	*RAP1GAP2*	-2.37	9.14E-52
LTC4S	**2.71**	**9.89E-22**	*MGC16275*	-2.32	1.58E-15
IER3	2.58	3.16E-19	*CCL3*	-2.30	2.39E-15
CLIC3	2.54	7.22E-207	*C5AR2*	-2.30	6.92E-38
SMAD7	2.48	7.13E-177	*SMIM35*	-2.21	4.05E-44
AC006033,2	2.47	8.08E-51	*SCAMP5*	-2.17	1.31E-89
NCR2	2.45	7.11E-15	*SEMA3G*	-2.16	1.94E-10
NKILA	2.45	2.82E-17	*CCR1*	-2.15	6.71E-46
CCL20	2.45	6.97E-14	*VEPH1*	-2.14	8.86E-11
SIAH3	2.44	1.77E-13	*CTLA4*	-2.13	7.23E-25
TINCR	2.38	6.31E-21	*TRABD2A*	-2.12	1.36E-22
LMO7	2.36	1.52E-52	*TNIP3*	-2.12	3.33E-11
SARDH	2.35	4.18E-13	*RPS27AP2*	-2.11	1.54E-12
RFX2	2.35	1.33E-170	*CSF2*	-2.10	2.48E-17
IL4I1	2.34	1.81E-16	*ITGA6*	-2.10	9.78E-33
LRRC2	2.34	1.68E-56	*FAM30A*	-2.06	8.34E-10
LINC00996	2.32	4.70E-21	*IGFBP7*	-2.05	1.03E-11
RASGRP3	2.32	1.14E-66	*RCN3*	-2.04	3.03E-11
GPR34	2.32	8.14E-27	*CREG2*	-2.04	1.57E-09
CPNE5	2.32	4.04E-25	*MUC1*	-2.03	1.78E-25
KCNH4	2.32	6.07E-19	*FAAHP1*	-2.03	5.49E-14
SKIL	2.30	7.28E-58	*WDR86-AS1*	-2.02	1.51E-21
FSCN1	2.28	2.04E-14	*EEPD1*	-2.00	4.88E-43
NXPH4	2.28	8.56E-14	*AC068279.2*	-1.99	4.20E-09
JAG2	2.27	1.42E-35	*PTGDS*	-1.98	5.46E-10
CYS1	2.24	4.05E-20	*AP003469.2*	-1.94	3.82E-13
FAM241A	2.21	8.62E-44	*AC061992.2*	-1.94	1.27E-08
UBE2QL1	2.21	3.48E-13	*HK3*	-1.93	1.51E-08
RGS1	2.20	6.30E-23	*NKG7*	-1.92	2.15E-52
TRGV8	2.20	6.33E-26	*BFSP1*	-1.91	2.59E-37
HS3ST1	2.19	2.27E-15	*SLC22A20P*	-1.90	1.89E-11
TRGV7	2.17	9.95E-33	*LINC00484*	-1.88	4.31E-11
CHST15	2.16	1.49E-10	*AC087645.2*	-1.86	2.72E-08
CCDC170	2.16	1.25E-10	*AC008894.2*	-1.85	5.31E-09
VASH1	2.15	4.89E-51	*RGS6*	-1.83	8.93E-10
CPNE7	2.14	5.19E-18	*HILPDA*	-1.83	1.22E-08
LTF	2.13	3.18E-10	*ITGA9*	-1.83	1.99E-10
PLEK2	2.11	4.23E-10	*AL355581.1*	-1.83	3.51E-10
KIF13A	2.09	8.07E-17	*GNG4*	-1.82	3.37E-09
TRO	2.07	1.89E-20	*CRISPLD2*	-1.82	1.01E-07
CYP4F22	2.05	7.93E-50	*SLC26A11*	-1.81	5.54E-14
PGLYRP2	2.04	5.08E-13	*WSCD2*	-1.79	4.52E-09
SMOX	2.01	3.85E-24	*SYNC*	-1.79	2.14E-07
DPY19L2	2.01	5.30E-10	*TMEM38A*	-1.78	1.54E-71
ATRNL1	2.01	3.04E-16	*HRH2*	-1.78	2.21E-07

412

TGFβ-induced natural ILC2 correlate with skin fibrosis

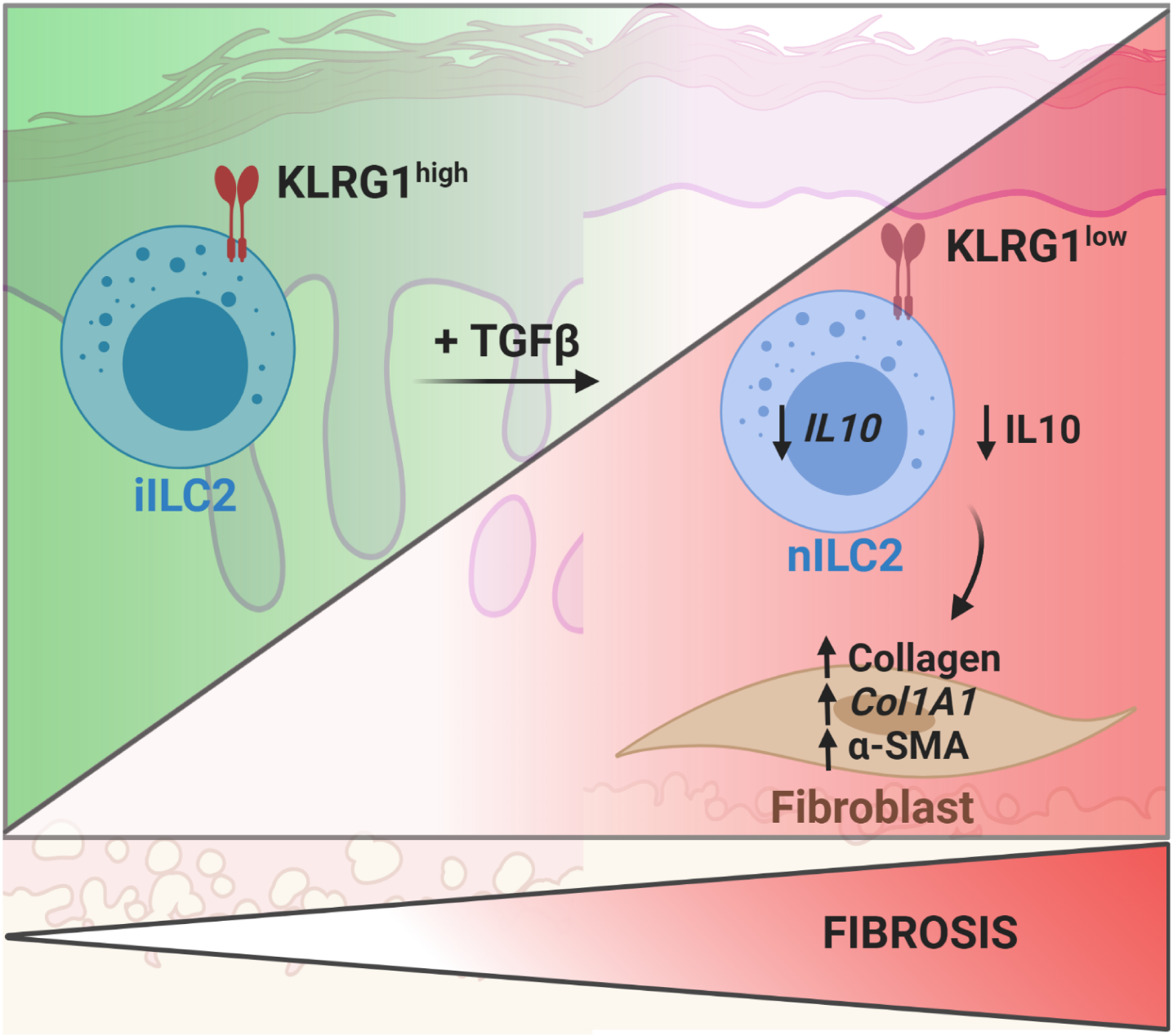

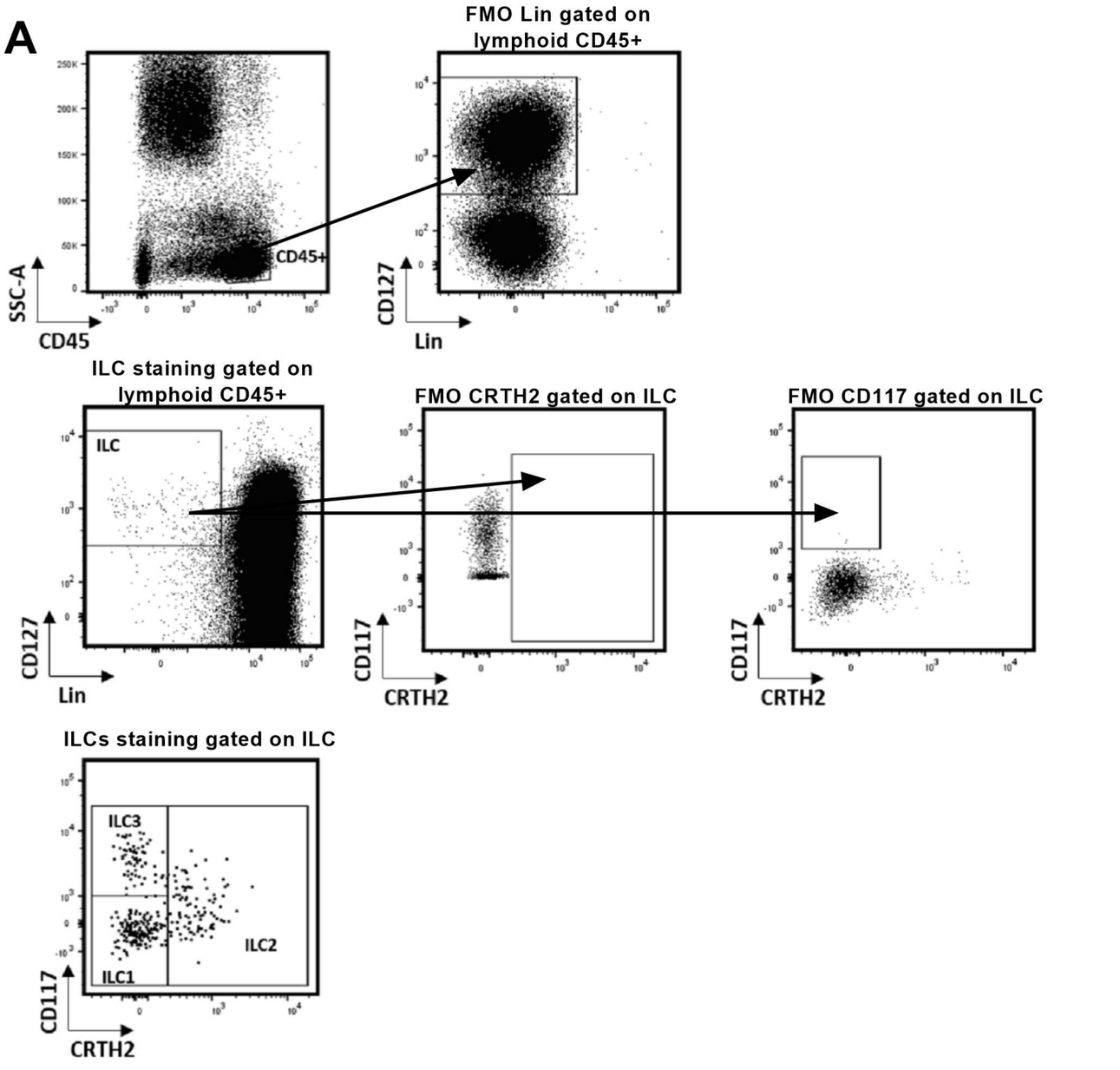
A
FMO Lin gated on lymphoid CD45+
SSC-A
CD45
CD45+
CD127
Lin
ILC staining gated on lymphoid CD45+
ILC
CD127
Lin
FMO CRTH2 gated on ILC
CD117
CRTH2
FMO CD117 gated on ILC
CD117
CRTH2
ILCs staining gated on ILC
ILC3
ILC2
ILC1
CD117
CRTH2
B
ILC staining gated on lymphoid CD45+
P1
P2
CD127
Lin
ILCs staining gated on P1
ILC3
39%
ILC2
ILC1
CD117
CRTH2
ILCs staining gated on P2
ILC3
21%
ILC2
ILC1
CD117
CRTH2

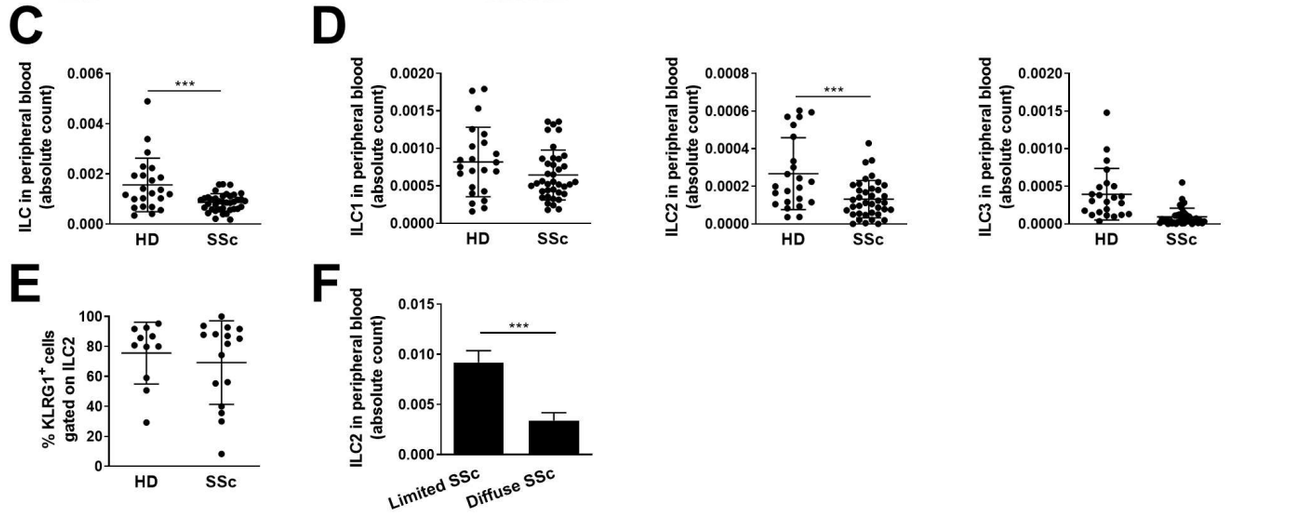
C
ILC in peripheral blood (absolute count)
***
HD
SSc
D
ILC1 in peripheral blood (absolute count)
HD
SSc
ILC2 in peripheral blood (absolute count)
***
HD
SSc
ILC3 in peripheral blood (absolute count)
HD
SSc
E
% KLRG1+ cells gated on ILC2
HD
SSc
F
ILC2 in peripheral blood (absolute count)
***
Limited SSc
Diffuse SSc

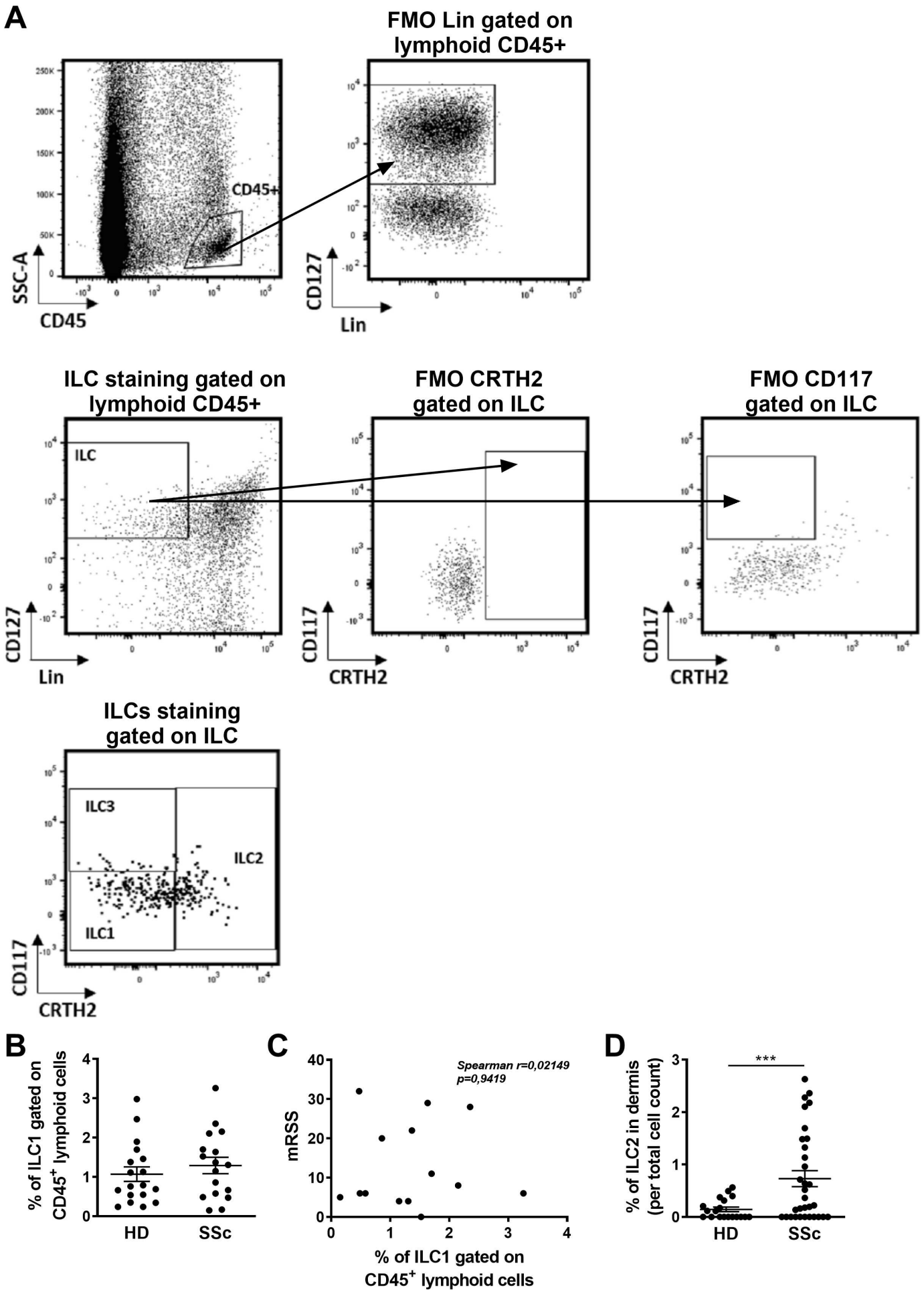
A
FMO Lin gated on lymphoid CD45+
CD45+
SSC-A
CD45
CD127
Lin
ILC staining gated on lymphoid CD45+
ILC
CD127
Lin
FMO CRTH2 gated on ILC
CD117
CRTH2
FMO CD117 gated on ILC
CD117
CRTH2
ILCs staining gated on ILC
ILC3
ILC2
ILC1
CD117
CRTH2
B
% of ILC1 gated on CD45+ lymphoid cells
HD
SSc
C
Spearman r=0,02149
p=0,9419
mRSS
% of ILC1 gated on CD45+ lymphoid cells
D
***
% of ILC2 in dermis (per total cell count)
HD
SSc

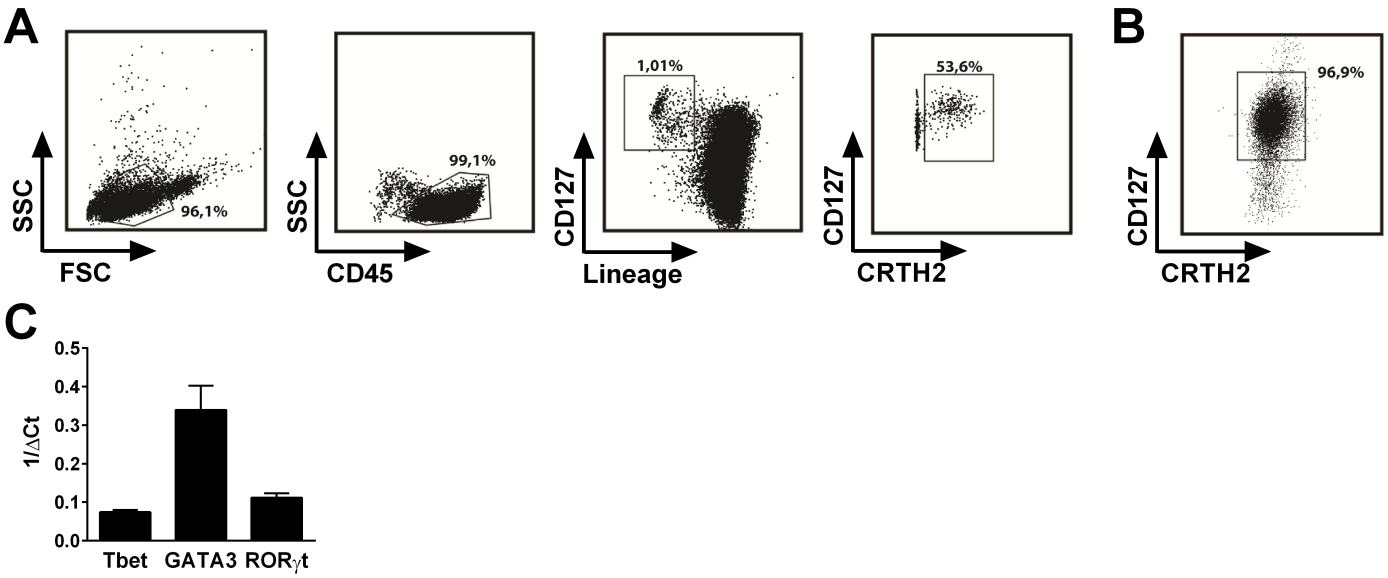
A
SSC
FSC
96,1%
SSC
CD45
99,1%
CD127
Lineage
1,01%
CD127
CRTH2
53,6%
B
CD127
CRTH2
96,9%
C
1/ΔCt
0.5
0.4
0.3
0.2
0.1
0.0
Tbet
GATA3
RORγt

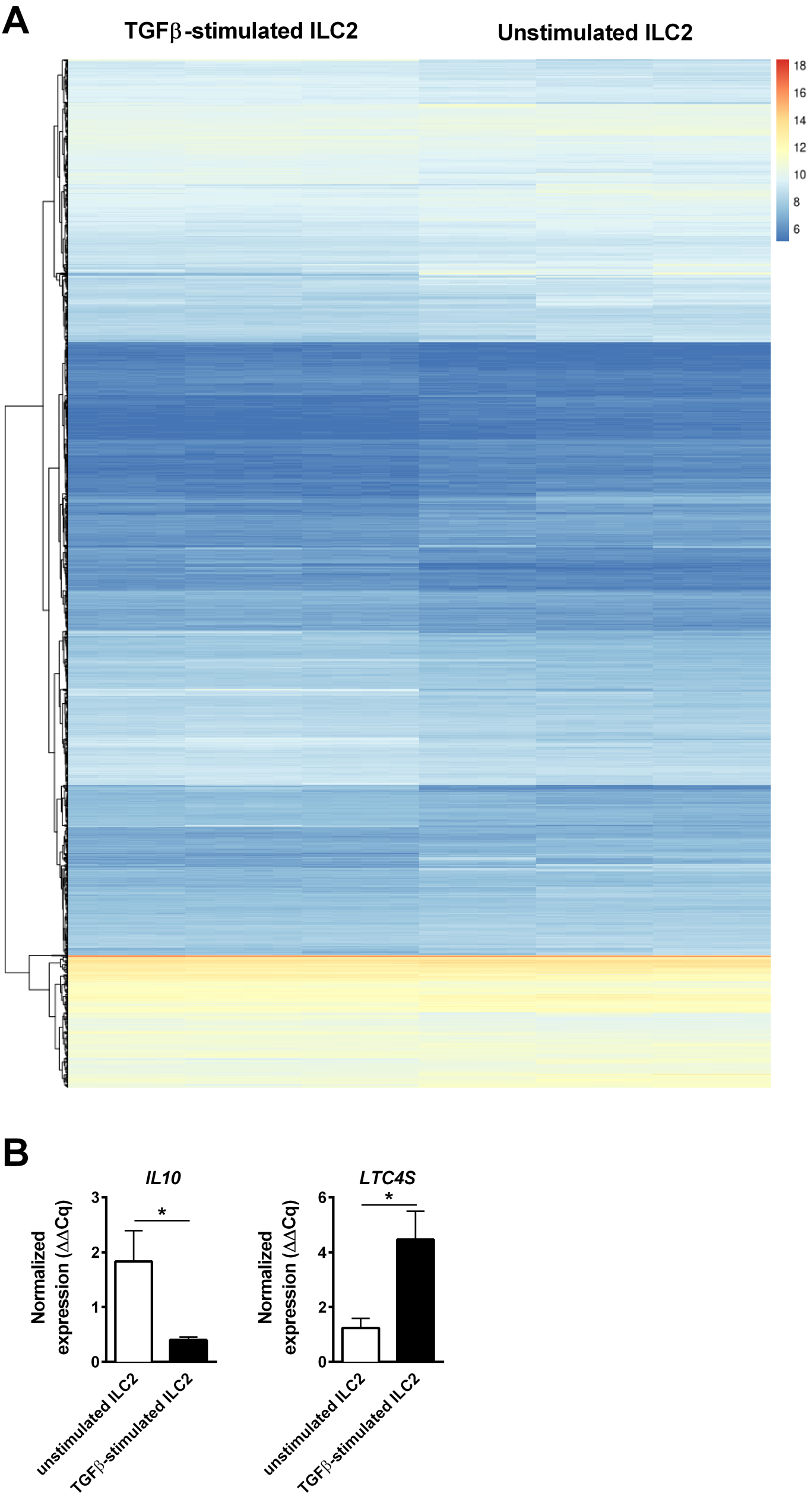
A
TGFβ-stimulated ILC2
Unstimulated ILC2
18
16
14
12
10
8
6
B
IL10
Normalized expression (ΔΔCq)
3
2
1
0
*
unstimulated ILC2
TGFβ-stimulated ILC2
LTC4S
Normalized expression (ΔΔCq)
6
4
2
0
*
unstimulated ILC2
TGFβ-stimulated ILC2

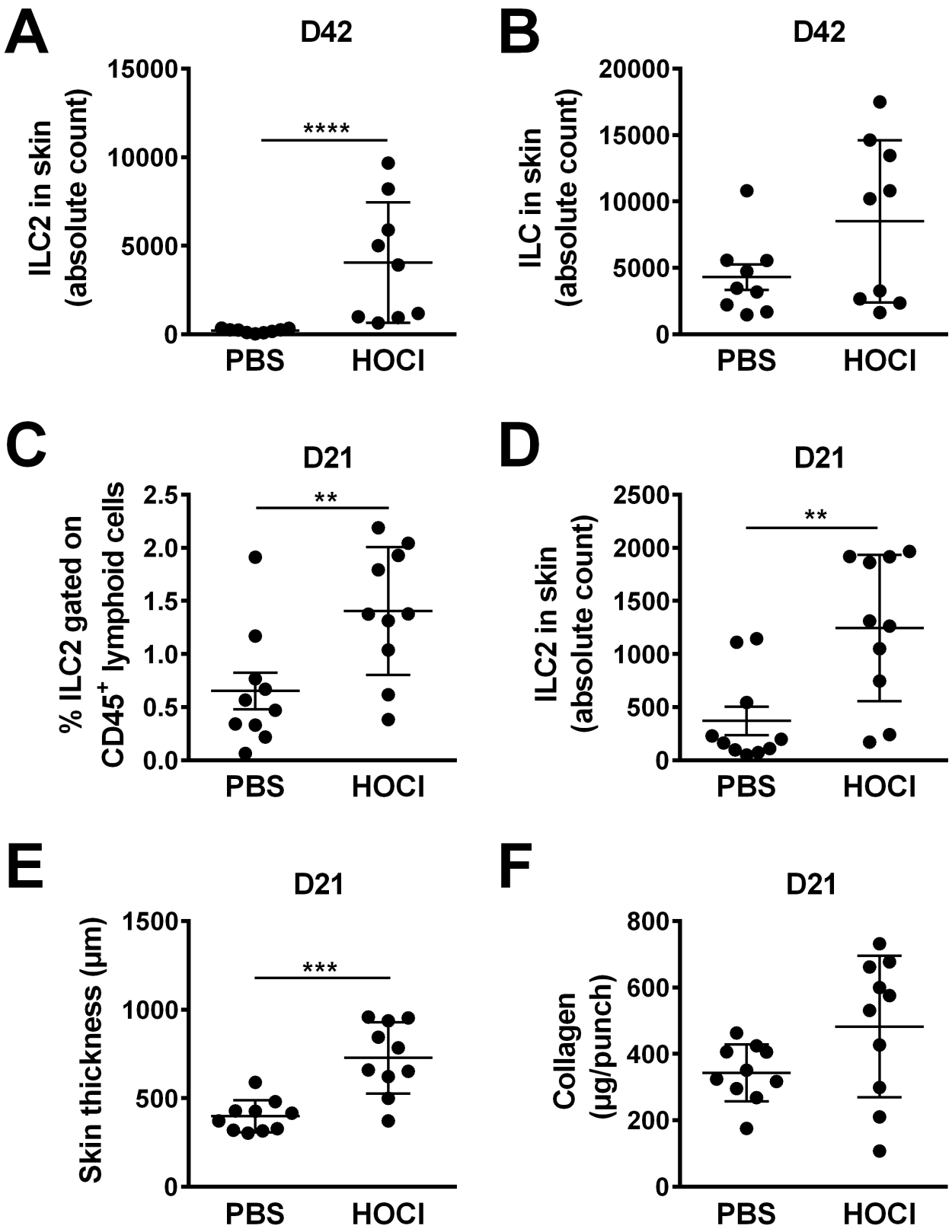
A
D42
ILC2 in skin (absolute count)
15000
10000
5000
0
****
PBS
HOCl
B
D42
ILC in skin (absolute count)
20000
15000
10000
5000
0
PBS
HOCl
C
D21
% ILC2 gated on CD45+ lymphoid cells
2.5
2.0
1.5
1.0
0.5
0.0
**
PBS
HOCl
D
D21
ILC2 in skin (absolute count)
2500
2000
1500
1000
500
0
**
PBS
HOCl
E
D21
Skin thickness (µm)
1500
1000
500
0
***
PBS
HOCl
F
D21
Collagen (µg/punch)
800
600
400
200
0
PBS
HOCl